

SPATIALALIGN: Aligning Dynamic Spatial Relationships in Video Generation

Fengming Liu¹ Tat-Jen Cham¹ Chuanxia Zheng¹

a fox is *on the right* of a stump, then the fox walks to the *left* of the stump. a squirrel is *on the right* of a rock, then the squirrel scampers to the *top* of the rock. a dog is *on the top* of a basket, then the dog jumps to the *left* of the basket.

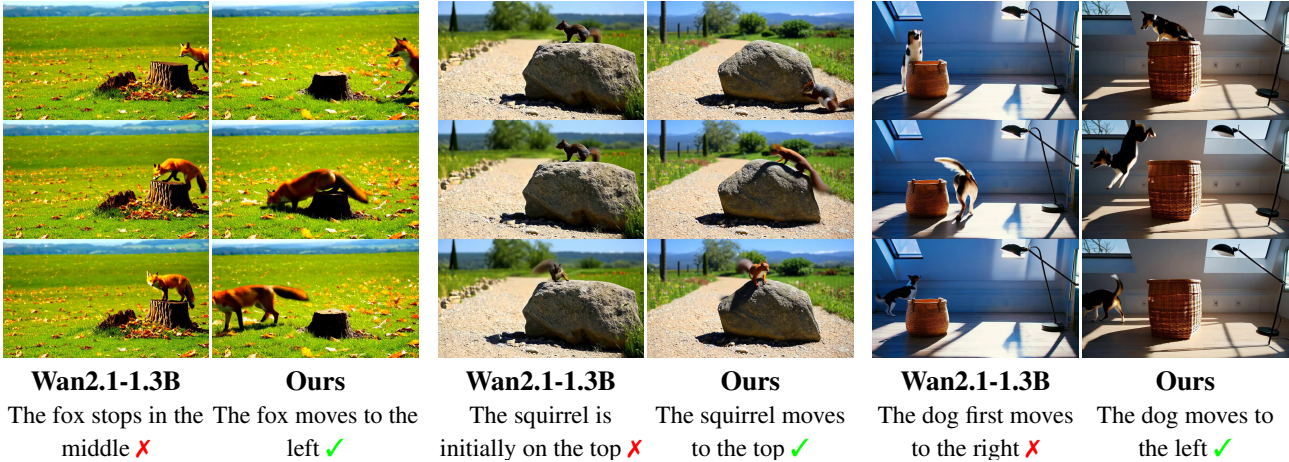


Figure 1. Examples of spatial relationship reasoning. Given a prompt specifying the spatial relationships (top), our fine-tuned model (right) generates videos that correctly reflect the desired change in spatial relationships, while the baseline model (left) fails to do so.

Abstract

Most text-to-video (T2V) generators prioritize aesthetic quality, but often ignoring the spatial constraints in the generated videos. In this work, we present SPATIALALIGN, a self-improvement framework that enhances T2V models’ capabilities to depict *Dynamic Spatial Relationships* (DSR) specified in text prompts. We present a zeroth-order regularized Direct Preference Optimization (DPO) to fine-tune T2V models towards better alignment with DSR. Specifically, we design DSR-SCORE, a geometry-based metric that quantitatively measures the alignment between generated videos and the specified DSRs in prompts, which is a step forward from prior works that rely on VLM for evaluation. We also conduct a dataset of text-video pairs with diverse DSRs to facilitate the study. Extensive experiments demonstrate that our fine-tuned model significantly outperforms the baseline in spatial relationships. The code will be released in [Link](#).

¹College of Computing and Data Science, Nanyang Technological University, 50 Nanyang Avenue, Singapore 639798. Correspondence to: Tat-Jen Cham <astjcham@ntu.edu.sg>.

1. Introduction

We live in a spatially and temporally structured world. When things move around and interact with the environment, we as humans often interpret these actions within the context of shared spatial relationships that change over time. A cat, for example, may first be sitting on the top of a table, and later moves to the right of it. Humans have a remarkable ability to understand, reason about, and even plan such spatial relationships. Likewise, developing similar capabilities in AI systems is crucial for a wide range of applications, like robotics, and physical world modeling (Chen et al., 2024).

We consider the task of generating plausible videos that accurately reflect *Dynamic Spatial Relationship* (DSR) instructions specified in text prompts. In particular, we introduce a simple yet representative task, where an *animal* moves with respect to a *static object*, leading to a change in the relative spatial relationship described in a prompt. For example, given the leftmost example in Figure 1, our goal is to generate a video where a fox first appears on the right side of the stump, and then moves to the left side. Surprisingly, we find that state-of-the-art T2V models (Wan et al., 2025; Yang et al., 2025b) often fail to capture such simple DSR instructions reliably.

Many recent contributions like GLIGEN (Li et al., 2023) and InstanceDiffusion (Wang et al., 2024) have shown promis-

ing results in modeling spatial control in generators, but these methods only work for *static* images and rely on extra inputs such as bounding boxes (bboxes). Instead, we ask *whether DSRs can be accurately scripted into generated videos from text prompts alone*. In this paper, we take an initial step towards realizing this goal, going beyond static spatial relationships in images.

Our first contribution is to develop **DSR-SCORE**, a metric to access the correctness of DSR in generated videos. The latest works like VBench-2.0 (Zheng et al., 2025), 3DSRBench (Ma et al., 2025a) and SpatialBench (Cai et al., 2025a) have proposed to use vision-language models (VLM) (Hurst et al., 2024; Bai et al., 2025) to evaluate such object-object spatial and temporal relationships over time. However, we find that VLM-based evaluation is not reliable in this task (as shown in Figure 4). This is partly due to the current VLMs’ limited spatial reasoning capabilities (Ma et al., 2025b;a; Batra et al., 2025), especially in dynamic settings. We thus propose to leverage *geometric* principles to design a more reliable and fine-grained evaluation metric for DSR. Spatial relationships (SR), for example “*on the left of*” or “*above*”, have clear geometric interpretations, which can be precisely defined and measured using bbox coordinates of the objects. In particular, by extracting the bbox using an off-the-shelf object detector and tracker (Ren et al., 2024), we compute the relative positions of the objects over time, and derive a DSR-SCORE that quantifies the degree of compliance with the DSR instructions.

Our second contribution is to introduce a novel training strategy, **SPATIALALIGN**, to enhance the DSR capability of pre-trained T2V models. A naïve approach would be to perform supervised fine-tuning (SFT) on real videos containing DSR scenarios. However, even if we collected such datasets, the SFT approach does *not* explicitly encourage the model to improve DSR alignment. The model may simply memorize training videos, without truly understanding the underlying SR. Instead, inspired by recent success in reinforcement learning from human feedback (RLHF) (Ouyang et al., 2022; Shao et al., 2024; Rafailov et al., 2023), we propose to leverage DSR-SCORE to provide feedback signals for self-improvement of the T2V model. In particular, we adopt **Direct Preference Optimization (DPO)** (Rafailov et al., 2023) to fine-tune the model on the generated videos labeled and paired with the DSR-SCORE. Our motivation for using DPO is two-fold: (1) DSR-SCORE is a non-differentiable numeric signal, which is not suitable for providing the direct gradient for SFT; (2) online RL methods such as PPO (Schulman et al., 2017) or GRPO (Shao et al., 2024) are computationally expensive, due to the need for doing multi-step diffusion inference online. By combining DSR-SCORE with DPO, we effectively provide a scalable and efficient way to enhance the DSR capability of T2V models, even without relying on real videos.

Finally, to evaluate our method, we built a new challenging benchmark **DSR-DATASET** of controlled DSR scenarios with diverse SR and motion patterns. We also conducted extensive experiments on multiple state-of-the-art T2V models, including CogVideoX (Yang et al., 2025b), LTX-Video (HaCohen et al., 2024), OpenSora (Peng et al., 2025), Wan2.1 (Wan et al., 2025) and HunyuanVideo 1.5 (Team, 2025b). Our results demonstrate that our proposed DSR-SCORE is more reliable than VLM-based metrics in evaluating DSR correctness, and our DPO-based training strategy effectively improves the DSR capability of T2V models, surpassing baseline methods by a large margin.

Although our study focuses on DSR, the problem formulation and solution are not limited to this specific task alone. In fact, our training strategy and evaluation metric offer greater value for physically-grounded video generation. The geometry-based formulation underlying the DSR-SCORE provides a general recipe for converting complex relational requirements into continuous, automatically computable signals, useful for a wide range of applications.

In summary, our key contributions are: (1) **DSR-SCORE**, a geometry-based metric for reliable evaluation of DSR in generated videos, which is more accurate and fine-grained than prior VLM-based approaches; (2) **SPATIALALIGN**, a DPO-based training strategy leveraging DSR-SCORE for aligning T2V models with DSR instructions, which outperforms SFT and other baselines significantly; and (3) **DSR-DATASET**, a new benchmark dataset for controlled evaluation of DSR in T2V models, along with extensive experiments demonstrating the effectiveness of our approach.

2. Related Work

Spatial Reasoning in Vision. Early works, like IQA (Gordon et al., 2018) and VQA (Wu et al., 2017), have explored spatial relationships in the context of visual question answering (VQA) tasks. More recently, SpatialVLM (Chen et al., 2024) and SpatialReasoner (Ma et al., 2025b) have focused on enhancing spatial reasoning capabilities in VLMs by incorporating 3D spatial annotations and explicit 3D representations, respectively. To evaluate the spatial reasoning abilities of VLMs, SpatialBench (Xu et al., 2025) has proposed a hierarchy of ability-oriented metrics. In the realm of T2V generation, the VBench series (Huang et al., 2024; Zheng et al., 2025) has introduced benchmarks for assessing DSR in generated videos. However, these evaluations primarily rely on vanilla VLMs, which are not reliable enough (Xu et al., 2025). Instead, we build a geometric-based evaluator by explicitly modeling spatial relationships.

Spatial Alignment in T2I and T2V Generation. Like our approach, spatially controlled generators aim to improve the spatial alignment between generated content and input prompts. GLIGEN (Li et al., 2023) pioneered this direction

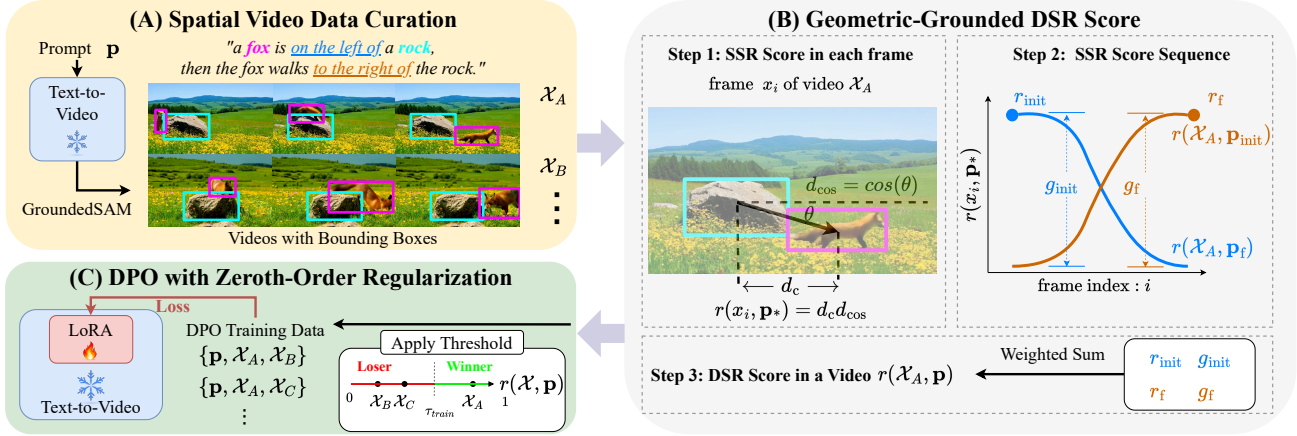


Figure 2. Overview of SPATIALALIGN. (A) Given a text prompt, the pre-trained T2V model generates several video samples. For each sample, we first use GroundedSAM to obtain the bboxes of the animal and the object in each frame. (B) Then, for each frame, we compute the Static Spatial Relationship (SSR) Score based on the bboxes. From the SSR Score Sequence (all frames), we derive four metric components that are aggregated into the DSR-SCORE, which quantifies how well the video aligns with the dynamic spatial relationship (DSR). (C) During DPO training, we identify winner/loser pairs based on the DSR-SCORE using a threshold. We then train a LoRA to enhance the model’s ability to accurately represent DSR in generated videos, using our proposed zero-order regularized DPO.

by introducing a gated self-attention layer to ground entities within specified bboxes. LayoutGPT (Feng et al., 2023) employs a training-free method that translates prompts into webpage code-like formats to dictate object layouts. BoxDiff (Xie et al., 2023) leverages text-to-latent cross-attention to enforce layout constraints during the denoising process. VideoTetris (Tian et al., 2024) decomposes prompts into frame-wise sub-prompts and region masks to enhance spatio-temporal consistency. DyST-XL (He et al., 2025) utilizes LLMs to interpret prompts and plan bboxes layouts, but its techniques are limited to specific architectures like MMDiT (Esser et al., 2024). Other works (Qi et al., 2024; Wu et al., 2024; Yang et al., 2024; Wang et al., 2025; Lian et al., 2023) directly modify latent representations to achieve desired layouts. However, they often depend on auxiliary controls, such as bboxes, masks, or layouts, to guide the SR. More importantly, most of these focus on “static” T2I generation, instead of “dynamic” T2V generation.

Preference Alignment in Generative models. Our method draws inspiration from DPO (Rafailov et al., 2023) and its diffusion adaptation Diffusion-DPO (Wallace et al., 2024), which optimize generators using paired preference data. These approaches bypass the need for online sampling, such as in PPO (Schulman et al., 2017) and GRPO (Shao et al., 2024), making them computationally efficient. More recently, this line of work has been extended to various diffusion-based generative models, including image generation (Na et al., 2025; Croitoru et al., 2025; Karthik et al., 2025), video generation (Liu et al., 2025; Yang et al., 2025a; Cai et al., 2025b), and 3D asset generation (Li et al., 2025). Our work is the first to apply DPO-based preference alignment to improve DSR reasoning in T2V generation.

3. Method

Given a pre-trained T2V generator p_{ref} that takes a text prompt \mathbf{p} as input and generates a video $\mathcal{X}_0 \sim p_{\text{ref}}(\mathcal{X}_0 | \mathbf{p})$, our goal is to learn a new T2V model p_θ that can generate videos with subjects moving in a manner that is more consistent with the dynamic spatial relationships described in the prompt \mathbf{p} , than the reference model p_{ref} .

As illustrated in Figure 2, our work consists of three key components: (1) we first collect a curated set of DSR prompts and generate videos using the reference T2V model p_{ref} ; (2) we then define and calculate DSR-SCORE, a novel metric to determine whether a video \mathcal{X}_0 is aligned with the DSR described in the prompt \mathbf{p} ; (3) finally, we fine-tune the T2V model p_θ using DPO (Rafailov et al., 2023), based on the preferences induced by DSR-SCORE.

3.1. Problem Definition and Preliminaries

Problem Definition and Notations. To simplify the problem, we focus on the DSR between an *animal* and a *static object*. For example, the sentence structure of a DSR prompt consists of a $\langle \text{scene} \rangle$, an $\langle \text{animal} \rangle$, a $\langle \text{static object} \rangle$, the $\langle \text{initial static spatial relationship (SSR)} \rangle$ and also the $\langle \text{final SSR} \rangle$, as shown in Figure 2. We present Table 1 to give a comprehensive overview of the initial/final SSRs and the corresponding *DSR type*. We further introduce a set of abstract notations – {LEFT, RIGHT, TOP} – as simplified representations for the “on the xxx of” DSR keyword phrases used in the following of the paper for brevity. In this paper, we explore DSRs formed by three types of SSRs: LEFT, RIGHT, and TOP, but our method is not specific to these and can be generalized to other types of DSRs.

	DSR Type	Initial SSR \mathbf{p}_{init}	Final SSR \mathbf{p}_{f}
A	left-to-top	on the left of	to the top of
B	top-to-left	on the top of	to the left of
C	right-to-top	on the right of	to the top of
D	left-to-right	on the left of	to the right of
E	top-to-right	on the top of	to the right of
F	right-to-left	on the right of	to the left of

Table 1. Overview of DSR types and the corresponding keywords.

In each video $\mathcal{X}_0 = \{\mathbf{x}_i\}_{i=1}^N$, where N is the number of video frames, we define the DSR as a transition from an initial static spatial relationship (SSR) to a final SSR, as summarized in Table 1. Specifically, for each frame \mathbf{x}_i , a corresponding SSR is defined as the spatial relationship between the $\langle \text{animal} \rangle$ and the $\langle \text{static object} \rangle$, which is common in *static* spatial T2I generators (Li et al., 2023; Feng et al., 2023). Due to the movement of the animal, the SSR will change over time. Although such a change is described in the prompt, the specific trajectory of the animal is *not* strictly defined, allowing for substantial variability.

Therefore, a key challenge in achieving DSR-aligned video generation is that it is difficult to define a precise optimization objective. In contrast, it is easy to determine whether a video \mathcal{X}_0 is aligned with the DSR described in the prompt \mathbf{p} by observing the change in SSR over time. Hence, we reformulate the problem as a *preference optimization task*, where the preference is induced by the alignment level with the DSR, which is quantified by our proposed DSR-SCORE.

Diffusion-DPO. As mentioned above, our goal is to optimize the T2V model p_θ based on the preferences induced by the reward score. The key idea is analogous to the T2I generator alignment in Diffusion-DPO (Wallace et al., 2024). It optimizes the diffusion model using the preference data, which is achieved by minimizing the following objective:

$$\mathcal{L}_{\text{DPO}} = -\mathbb{E}_{(\mathbf{x}_0^w, \mathbf{x}_0^l) \sim D, t \sim \mathcal{U}(0, T), \mathbf{x}_t^w \sim q(\mathbf{x}_t^w | \mathbf{x}_0^w), \mathbf{x}_t^l \sim q(\mathbf{x}_t^l | \mathbf{x}_0^l)} \left(\log \text{sigmoid} \left(-\beta T w(\lambda_t) \left(\|\epsilon^w - \epsilon_\theta(\mathbf{x}_t^w, t)\|_2^2 - \|\epsilon^w - \epsilon_{\text{ref}}(\mathbf{x}_t^w, t)\|_2^2 - (\|\epsilon^l - \epsilon_\theta(\mathbf{x}_t^l, t)\|_2^2 - \|\epsilon^l - \epsilon_{\text{ref}}(\mathbf{x}_t^l, t)\|_2^2) \right) \right) \right), \quad (1)$$

where $\mathbf{x}_t^* = \alpha_t \mathbf{x}_0^* + \sigma_t \epsilon^*$, with $\epsilon^* \sim \mathcal{N}(0, \mathbf{I})$, and $*$ $\in \{w, l\}$ denotes the ‘‘winner’’ and ‘‘loser’’ samples, respectively. Here, ϵ_θ and ϵ_{ref} are the noise prediction networks of the fine-tuned and reference diffusion models, respectively. T is the total number of diffusion steps, and β is a hyperparameter that controls the strength of the preference optimization. $w(\lambda_t)$ is an important weight function. Please refer to (Wallace et al., 2024) for more details.

3.2. Geometric-Grounded DSR-SCORE

The key to the success of DPO training is to define a reliable reward metric that can plausibly reflect the level of alignment with the DSR described in the prompt. Existing spatial reasoning works (Ma et al., 2025b;a; Cai et al., 2025a) often rely on VLMs (Hurst et al., 2024; Bai et al., 2025) to evaluate the correctness of spatial relationships. However, as we will discuss in Section 3.5, such a VLM-based evaluation can be unreliable and inaccurate. To address this issue, we propose a novel geometrically based metric, termed DSR-SCORE, to quantify the alignment level with the DSR.

Static Spatial Relationship (SSR) Score in each frame.

Given a video $\mathcal{X}_0 = \{\mathbf{x}_i\}_{i=1}^N$, we first define the SSR-Score $r(\mathbf{x}_i, \mathbf{p}_*) \in [-1, 1]$ to quantify the alignment level of each frame \mathbf{x}_i with a specific SSR \mathbf{p}_* expressed by the prompt \mathbf{p} , where $\mathbf{p}_* \in \{\text{LEFT}, \text{RIGHT}, \text{TOP}\}$.

As illustrated in Figure 2 (b) on the left, the SSR-Score is computed based on the spatial relationship between the bboxes b_a and b_o of the animal and the static object, which are obtained using GroundedSAM (Ren et al., 2024). Then, the SSR-Score is defined as the product of two quantities:

$$r(\mathbf{x}_i, \mathbf{p}_*) = d_c(b_a, b_o) d_{\cos}(b_a, b_o), \quad (2)$$

where $d_c(b_a, b_o) = \text{clip}(|\frac{b_a^{c*} - b_o^{c*}}{(b_a^{c*} + b_o^{c*})/2}|, 0, 1)$ is the normalized distance between the centers of the two bboxes along the relevant axis ($*$ is the placeholder that takes ‘‘ x ’’ for LEFT/RIGHT and ‘‘ y ’’ for TOP, b_*^{c*} denotes the center coordinate along the relevant axis, and b_*^* denotes the width/height of the bbox along that axis); and $d_{\cos}(b_a, b_o)$ is the cosine distance between the object-to-animal center-based vector $v(b_a, b_o)$ and the axis. The second term is necessary to ensure that the two entities are indeed positioned in the specified spatial relationship. For example, for the LEFT SSR, the object-to-animal vector should predominantly be aligned in the horizontal direction, with a relatively small vertical component.

In a video generated with a prompt defining an initial SSR \mathbf{p}_{init} and a final SSR \mathbf{p}_{f} , the actual SSR for each successive frame should change. To better understand this transition, we can use the SSR-Score to separately assess the alignment of each frame to both the initial and final prompted SSRs. For example, suppose $\mathbf{p}_{\text{init}} = \text{LEFT}$ and $\mathbf{p}_{\text{f}} = \text{TOP}$, then if our SSR-Score reports $r(\mathbf{x}_i, \text{LEFT}) = 0.7$, it means that \mathbf{x}_i satisfies LEFT at the level of 0.7, while if $r(\mathbf{x}_i, \text{TOP}) = 0.2$, it means that \mathbf{x}_i satisfies TOP at the level of 0.2. This approach helps to generalize the understanding of SSR to the whole video. Specifically, the alignment to SSR \mathbf{p}_* of video \mathcal{X}_0 can be described by the *SSR-Score sequence* $\{r(\mathbf{x}_i, \mathbf{p}_*)\}_{i=1}^N$, which is a list of per-frame SSR-Scores.

Dynamic Spatial Relationship (DSR) Score in one video.

The DSR-SCORE $r(\mathcal{X}_0, \mathbf{p})$ is then defined based on the SSR-Scores sequence over all frames in \mathcal{X}_0 . As illustrated in Figure 2 (b) right, an ideal video sample should exhibit a “crossing” pattern between the SSR-Score curves of the initial and final SSRs over time. This is because, as the animal moves according to the DSR, the alignment level with the initial SSR \mathbf{p}_{init} should decrease, while the alignment level with the final SSR \mathbf{p}_f should increase. To capture this intuition, the DSR-SCORE is defined as follows:

$$r(\mathcal{X}_0, \mathbf{p}) = 0.125(r_{\text{init}} + r_f + g_{\text{init}} + g_f) + 0.5, \quad (3)$$

where 0.125 and 0.5 are used for normalization to ensure that the DSR-SCORE lies in $[0, 1]$, where a higher score indicates better alignment with the DSR. Here, $r_{\text{init}} = \frac{1}{m} \sum_{k=1}^m r(\mathbf{x}_k, \mathbf{p}_{\text{init}})$ and $r_f = \frac{1}{m} \sum_{k=N-m+1}^N r(\mathbf{x}_k, \mathbf{p}_f)$ are the average SSR-Scores of the first and last m frames, respectively, which reflect the alignment quality with the initial and final SSRs at the two ends of the video. Additionally, $g_{\text{init}} = r(\mathbf{x}_1, \mathbf{p}_{\text{init}}) - r(\mathbf{x}_N, \mathbf{p}_{\text{init}})$ and $g_f = r(\mathbf{x}_N, \mathbf{p}_f) - r(\mathbf{x}_1, \mathbf{p}_f)$ are the absolute differences between the SSR-Scores of the start and end frames, which reflects the extent of transition.

3.3. Spatial-Aligned Video Data Curation

As shown in Figure 2 (a), we first generate samples using the reference T2V model p_{ref} . Before we reward these videos using our DSR-SCORE, we first curate these samples to ensure that they are **VALID**. Specifically, we use a grounded object tracking model (Ren et al., 2024) to track the bboxes of the animal and the static object in each generated video. We then filter out the video samples that do not satisfy the following criteria: (1) There is only **One** animal and **One** describing static object as designated in the prompt; and (2) The two entities are successfully detected in at least 20 frames. Then, we compute the DSR-SCORE $r(\mathcal{X}_0, \mathbf{p})$ for each valid video \mathcal{X}_0 . We use a threshold τ_{train} to divide the video samples under each prompt \mathbf{p} , where the samples with $r(\mathcal{X}_0, \mathbf{p}) \geq \tau_{\text{train}}$ are labeled as winners, otherwise losers. Note that, the existence of invalid samples is also an important reason why online RL methods such as PPO and GRPO are not applicable, since their reward on an invalid sample can not provide meaningful signal for optimization.

3.4. DPO with Zeroth-Order Regularization

We can now fine-tune the T2V model p_θ with the curated data using the DPO loss defined in Equation (1). In particular, we treat the positive samples as the “winner” samples \mathcal{X}_0^w and the negative samples as the “loser” samples \mathcal{X}_0^l for each prompt \mathbf{p} . We follow the LoRA technique to efficiently fine-tune the T2V model. However, directly applying DPO training to our situation leads to degraded results, which is termed *likelihood displacement* (Pal et al., 2024; Pang

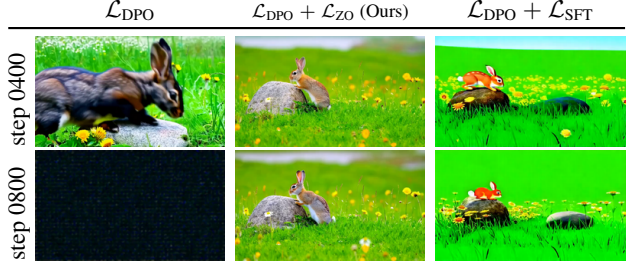


Figure 3. **Ablation on loss.** With only the DPO loss \mathcal{L}_{DPO} , the model degrades after 800 steps. With SFT loss \mathcal{L}_{SFT} , the color saturation is strong. With our zeroth-order regularization \mathcal{L}_{ZO} , the training is stable.

et al., 2024; Razin et al., 2025). As shown in Figure A7 in Appendix A2, the DPO loss satisfies the margin by degrading the performance on both the winner and the loser, by forcing a much poorer performance on the losing side.

We attribute this issue to the nature of the DSR problem. Essentially, DSR are high-level concepts, which are not directly reflected in the pixel values (in comparison, other properties such as aesthetics may be more closely linked to pixel values). Purely using DPO loss may lead the model to learn *shortcuts* to satisfy the margin in an unintended way. To address this issue, we introduce an additional loss term to further regularize the fine-tuned model. First, we naïvely combine the supervised fine-tuning (SFT) loss with the DPO loss:

$$\mathcal{L} = \mathcal{L}_{\text{DPO}} + \lambda_{\text{SFT}} \mathcal{L}_{\text{SFT}}, \quad (4)$$

where $\mathcal{L}_{\text{SFT}} = \|\epsilon^w - \epsilon_\theta(\mathcal{X}_t^w, t)\|_2^2 + \|\epsilon^l - \epsilon_\theta(\mathcal{X}_t^l, t)\|_2^2$, and λ_{SFT} is a hyperparameter. This simple combination helps to stabilize the training process and improve the DSR alignment, but leads to sub-optimal results with over-saturation issues (as shown in Figure 3). To further mitigate this issue, we introduce a *Zeroth-Order* regularization term in addition to the *First-Order* DPO loss,

$$\mathcal{L} = \mathcal{L}_{\text{DPO}} + \lambda_{\text{ZO}} \mathcal{L}_{\text{ZO}}, \quad (5)$$

where $\mathcal{L}_{\text{ZO}} = \|\epsilon_{\text{ref}}(\mathcal{X}_t^w, t) - \epsilon_\theta(\mathcal{X}_t^w, t)\|_2^2 + \|\epsilon_{\text{ref}}(\mathcal{X}_t^l, t) - \epsilon_\theta(\mathcal{X}_t^l, t)\|_2^2$, and λ_{ZO} is a hyperparameter. This regularization considers the reference model as an anchor point, which avoids the “reward hacking” issue where *shortcuts* are learned to reduce preference loss, but actually leads to the generation quality deviating excessively from those produced by the reference model.

3.5. Reliability of VLM for Assessing DSRs

To better understand the advantages of our proposed DSR-SCORE, we tested with Qwen3-VL-8B-Instruct (Team, 2025a) as the VLM-based metric (Ma et al., 2025a) for DSR evaluation, in accordance with popular practice. Fol-

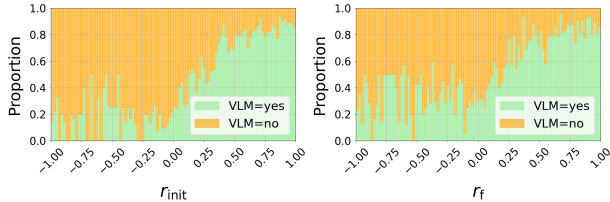


Figure 4. **VLM vs DSR-SCORE**. Each plot contains bins at each SSR Score value. Each bin shows the portion where the VLM gives the **YES** answer or **NO** answer at the particular SSR Score location. The VLM gives a significant portion of **YES** on the low SSR Score interval, especially for the evaluation on the final SSR.

lowing VBench-2.0 (Zheng et al., 2025), we designed two questions for the initial SSR and the final SSR, respectively:

- (1) *Is the \langle animal \rangle initially \langle initial SSR \rangle the \langle object \rangle ? Answer yes or no.*
- (2) *Is the \langle animal \rangle finally \langle final SSR \rangle the \langle object \rangle ? Answer yes or no.*

We collected the YES/NO answers given by the VLM and correlate them with the SSR-Scores of the initial SSR and the final SSR on a large set of videos.

Figure 4 shows the correlation plots of VLM answers vs DSR-SCORES. As formulated in Section 3.2, $r_{\text{init}} / r_{\text{f}}$ reflects the level of alignment to the initial/final SSR of the video. However, the plots show that the VLM gives a non-negligible portion of YES answers on videos with low scores. This surprisingly shows that the VLM tends to provide positive responses regardless of the actual spatial relationship in the video. Nonetheless, we comparatively evaluated the use of VLM answers as the reward for training, and the details are discussed in Section 4.3.

4. Experiments

4.1. Settings

Dataset. We conducted experiments on our curated dataset named DSR-DATASET, designed for training and evaluating T2V models on DSR prompts. For training, we collected 500 DSR prompts using GPT-4o, each accompanied by 10 video samples generated with random seeds. For testing, we curated 120 DSR prompts, each evaluated with 5 fixed seeds to ensure reproducibility. Note that, (1) only **VALID** samples are involved in the training; and (2) the exact DSR-SCORE value is not involved for DPO training. More details about the dataset are provided in Appendix A1.2.

Metrics. For quantitative results, we report the **Correctness@0.7** metric, ID Consistency, CLIP-IQA (Wang et al., 2023), and Imaging Quality. Correctness@0.7 indicates the percentage of generated videos achieving an DSR-SCORE

Method	Correct@0.7 \uparrow	ID \uparrow	CLIP-IQA \uparrow	IQ \uparrow
CogVideoX1.5-5B	0.053	0.6404	0.8874	0.5894
OpenSora v1.2	0.018	0.7151	0.8712	0.6616
LTX-Video-2B	0.058	0.8028	<u>0.9061</u>	0.6786
HunyuanVideo v1.5-8B	<u>0.490</u>	<u>0.7565</u>	0.9299	0.6662
Wan2.1-1.3B	0.125	0.7046	0.8481	0.7000
Wan2.1-1.3B + LoRA (Ours)	0.585	0.6934	0.8243	<u>0.6909</u>

Table 2. **Quantitative Results on DSR-DATASET**. “Correct@0.7” denotes Correctness at threshold 0.7. “ID” denotes ID Consistency. “CLIP-IQA” denotes CLIP-based Image Quality Assessment. “IQ” denotes Imaging Quality. The best and second-best results are **bolded** and underlined, respectively. Our method achieves the best correctness while maintaining decent image quality.

value greater than or equal to 0.7, reflecting the model’s ability to align with DSR prompts. ID Consistency measures the consistency of the animal appearance along the video frames, by extracting DINOv2 features (Oquab et al., 2023) on the bbox area containing the animal. CLIP-IQA and Imaging Quality collectively assess the visual quality of the generated samples. Limited by space, more details about the metrics are provided in Section A1.

Implementation Details. SPATIALALIGN is mainly trained with the Wan2.1-1.3B (Wan et al., 2025) T2V model. However, our method is architecture-agnostic and can be applied to a wide range of I2V models. We fine-tune two prompt-related components using LoRA (Hu et al., 2022): (1) the projection module mapping text embeddings into the model’s latent space, and (2) the key and value projection matrices in every cross-attention layer. The video consists of 81 frames at 480×832 resolution. We use AdamW (Loshchilov & Hutter, 2017) to fine-tune the model with LoRA at rank 16. The learning rate is $1e-4$. The batch size is 48 and the training is conducted for 2400 steps on 4 RTX4090’s. We set $\beta = 1$ in the DPO loss and $\lambda_{ZO} = 0.25$. More details are provided in Section A1.

4.2. Main Results

Quantitative Results. We compare SPATIALALIGN to the state-of-the-art T2V models in Table 2, including OpenSora 2.0 (Peng et al., 2025), CogVideoX1.5-5B (Yang et al., 2025b), Wan2.1-1.3B (Wan et al., 2025), LTX-Video-2B (HaCohen et al., 2024), and HunyuanVideo1.5-8B (Team, 2025b). SPATIALALIGN significantly outperforms these baselines in Correctness@0.7, demonstrating its effectiveness in generating videos that are better aligned with DSR prompts. The detailed *correctness curve* is shown in Figure A6a, showing how SPATIALALIGN consistently improves correctness across various thresholds. For the other metrics, SPATIALALIGN maintains comparable ID Consistency, visual quality and Image Quality to the baseline Wan2.1-1.3B, demonstrating that the fine-tuning does not compromise these aspects. Note that, HunyuanVideo1.5-

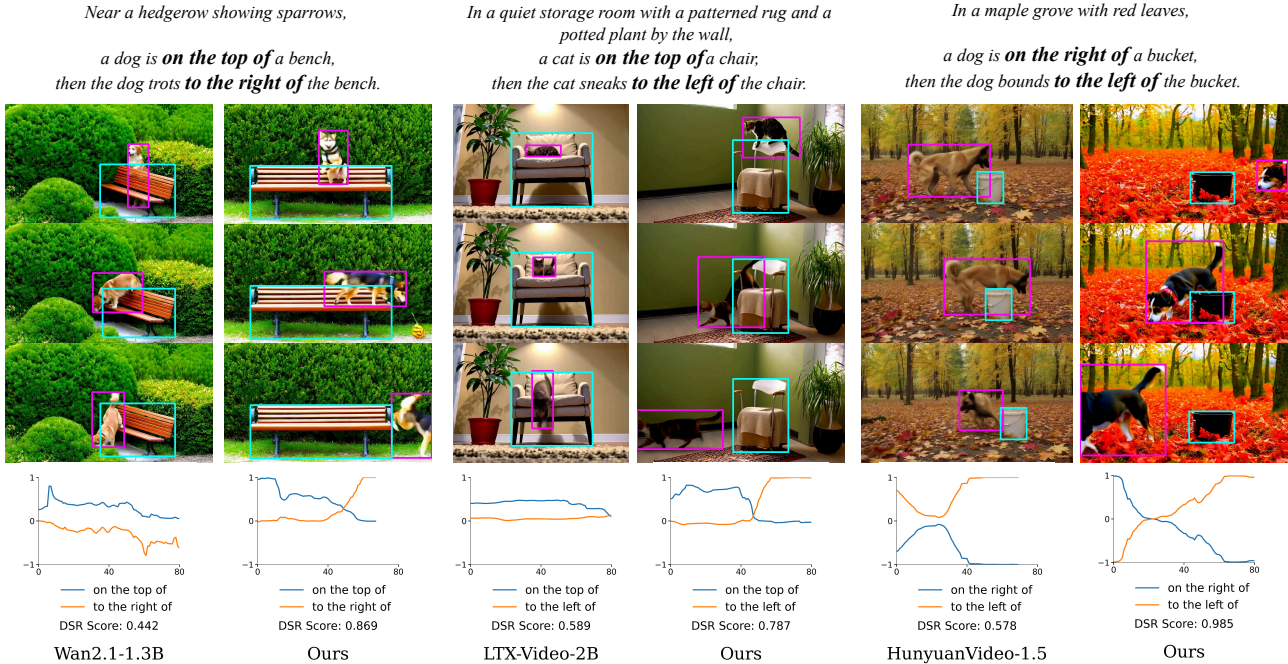


Figure 5. Qualitative comparisons with the state-of-the-art T2V models on DSR-DATASET. Our fine-tuned model (right columns) generates videos that correctly reflect the desired change in spatial relationships, while the baseline models (left columns) fail to do so.

8B achieves the second best ID Consistency and the best CLIP-IQA score, likely attributed to its larger model size.

Qualitative Results. SPATIALALIGN outputs are visually compared with the latest T2V models in Figure 5. SPATIALALIGN generates videos that accurately reflect the spatial dynamics described in the DSR prompts, while maintaining high visual fidelity. In contrast, the baseline and other SOTA models often fail to capture the correct spatial relationships, resulting in less coherent videos.

4.3. Ablations

We conducted thorough ablations on various components of our method, as summarized in Table 4. Due to resource constraints, all ablations were performed with 800 training steps and on a subset of 500 training prompts and 30 testing prompts, unless specified otherwise.

Training loss. The DPO training serves as a cornerstone to the success of SPATIALALIGN, as it is hard to directly supervise spatial relationship alignment. To validate this, we compare our default DPO training with two alternatives in Table 3a: (1) supervised fine-tuning (SFT) using the top-2-DSR-SCORE samples, and (2) DPO without a global threshold τ_{train} , where the winner/loser pairs are randomly sampled based on their relative DSR-SCORE values. The results show that our DPO with a global threshold outperforms both alternatives, highlighting the effectiveness of

our training strategy. Note that SFT-based methods lead to significant degradation in visual quality, as indicated by the low CLIP-IQA “natural” score, even if supervised by high-DSR-SCORE samples. We also compared the alternative SFT regularization loss to our zeroth-order regularization loss \mathcal{L}_{Z0} . Note that with more training steps (2,400 steps), our DPO with \mathcal{L}_{Z0} outperforms the SFT-based method in all metrics (Figure A8b). More importantly, the SFT-based supervision or regularization suffers from color saturation issues, resulting in unrealistic video appearances (Figure 3).

Reward System. Our geometry-based DSR-SCORE is significant in providing a reliable reward system for DSR alignment. We investigated by comparing with two VLM-based reward systems in Table 3b: (1) Qwen3-VL-8B-Instruct (Team, 2025a), and (2) VBench-2.0 (Zheng et al., 2025). When trained with these VLM-based rewards, the spatial correctness is not only significantly lower than using our DSR-SCORE, but is even worse than the baseline without fine-tuning (Table 3c), indicating that VLM-based spatial judgment is unreliable for use as a reward signal.

DSR-SCORE Component. We further ablate the components of DSR-SCORE in Table 3b. Specifically, we remove the gap values g_{init}, g_f from DSR-SCORE and only use the endpoint values r_{init}, r_f as reward scores. The results show that removing the gap values leads to degraded performance, indicating that including information on the transition process is important for overall performance enhancement.

(a) **Training loss.** SFT with top-2 samples brings limited improvement. Removing τ degrades the performance significantly.

Method	Correct@0.7 \uparrow	ID \uparrow	CLIP-IQA \uparrow	IQ \uparrow
SFT, top-2	0.187	0.7549	0.6330	0.7113
DPO, no τ_{train}	0.113	0.7102	0.8667	0.7298
$\mathcal{L}_{DPO} + \mathcal{L}_{SFT}, \tau_{train} = 0.7$	0.333	0.7317	0.6549	0.7107
$\mathcal{L}_{DPO} + \mathcal{L}_{ZO}$ (Ours)	0.307	0.6754	0.8594	0.7141

(c) **Threshold** τ_{train} for splitting winner/loser data. Large τ_{train} leads to better spatial correctness, but worse video quality.

Method	Correct@0.7 \uparrow	ID \uparrow	CLIP-IQA \uparrow	IQ \uparrow
Wan2.1-1.3B (Baseline)	0.180	0.6935	0.8723	0.7293
0.6	0.200	0.7152	0.8635	0.7335
0.7 (Ours)	0.307	0.6754	0.8594	0.7141
0.8	0.367	0.6466	0.8401	0.7153

Table 4. **SPATIALALIGN Ablations.** All models are fine-tuned for 800 steps unless specified otherwise. Results are evaluated on a subset of 30 test prompts. The best results are **bolded**.

Ablations on threshold τ_{train} . The default threshold of $\tau_{train} = 0.7$ is used for splitting winner/loser training samples. We ablate the choice of τ_{train} in Table 3c and Figure A8d. With $\tau_{train} = 0.6$, the model is unable to significantly improve spatial correctness. Conversely, with $\tau_{train} = 0.8$, the model gives a higher performance on spatial correctness, showing that a higher τ_{train} enhances the signal-to-noise ratio for winner/loser pairs. Evidently our DSR-SCORE is effective in assessing spatial alignment and can serve as a reliable reward signal. However, a higher τ_{train} leads to a lower CLIP-IQA “natural” score, indicating degraded naturalness in visual appearance. This can be explained by the decreasing percentage of available training data, since a higher τ_{train} filters out more winner training samples. Thus, there is a trade-off in selecting τ_{train} .

Ablations on different prompt structure. Another important question is whether the effectiveness of our method is sensitive to the prompt structure. To test the prompt generalizability of our method, we test our fine-tuned model on alternative structures of DSR prompts (Table 3d). We tested three ablations: (1) augmenting the prompt with ChatGPT (Hurst et al., 2024), (2) likewise with Qwen2.5-7B-Instruct (Bai et al., 2025), and (3) modifying the prompt into a “from ... to ...” structure, such as “a fox is on the left of a chair, then the fox sprints to the right of the chair” being rephrased as “a fox sprints from the left of a chair to the right of the chair”. For fair comparison, we used the same model fine-tuned on **our structured prompt** for testing on all three alternative prompt structures. Across all these alternative prompts, the fine-tuned model performs better than the baseline, suggesting that the fine-tuned model has learned deeper semantic knowledge about spatial relationships, beyond simply overfitting to prompt structure.

(b) **Reward system.** Our DSR-SCORE outperforms Qwen3-VL-8B and VBench-2.0 significantly on spatial correctness.

Method	Correct@0.7 \uparrow	ID \uparrow	CLIP-IQA \uparrow	IQ \uparrow
Qwen3-VL-8B-Instruct	0.147	0.7269	0.8746	0.7268
VBench-2.0	0.147	0.7435	0.8738	0.7301
Endpoint SSR	0.180	0.7243	0.8750	0.7240
DSR-SCORE (Ours)	0.307	0.6754	0.8594	0.7141

(d) **Different form of prompt.** Our method consistently outperforms the baseline under different prompt forms.

Augmentation	Method	Correct@0.7 \uparrow	ID \uparrow	CLIP-IQA \uparrow	IQ \uparrow
ChatGPT	baseline	0.107	0.6621	0.8626	0.7176
	Ours	0.407	0.6816	0.8461	0.7039
Qwen2.5	baseline	0.180	0.6994	0.8511	0.7033
	Ours	0.433	0.7231	0.8402	0.6884
from ... to ...	baseline	0.107	0.5967	0.8602	0.7125
	Ours	0.367	0.6345	0.8423	0.6954

5. Conclusion

We present SPATIALALIGN, a self-improvement framework for enhancing T2V generators in modeling dynamic spatial relationships (DSR). The key to our success is that we construct a zero-order DPO reward function to fine-tune the T2V models towards better alignment with DSR. Unlike prior works that rely on VLMs for evaluating spatial relationships, we propose a geometry-based DSR-SCORE metric to provide more reliable and interpretable measurement of DSR alignment. The resulting model demonstrates a significant improvement in generating videos that accurately reflect the dynamic spatial relationships specified in the text prompts, where preserve the identity and image quality. The simplicity and efficiency of our approach also make it a potentially promising solution for enhancing T2V models in other high-level physical attributes beyond DSR.

Limitations and Discussions. Despite the promising results, SPATIALALIGN has some limitations. First, the calculation of the geometry-based DSR-SCORE is highly dependent on the robustness of GroundedSAM (Ren et al., 2024). However, it does not always perform perfectly, especially for generated videos with complex scenes and motion blur. These defects can lead to incorrect DSR-SCORE values or even invalid samples. A more robust detection and tracking tool should be adopted for a more reliable DSR-SCORE system. Second, our work only explores the setting of one animal and one object with DSRs on LEFT, RIGHT, and TOP. More complicated settings, such as a scene graph, should be explored to prove the generalizability of our design of the reward on dynamic spatial relationships.

Acknowledgments. This research is supported by the Ministry of Education, Singapore, under its Academic Research Fund Tier 1 RG107/24. Chuanxia Zheng is supported by NTU SUG-NAP and the National Research Foundation, Singapore, under its NRF Fellowship Award NRF-NRFF17-2025-0009.

References

- Bai, S., Chen, K., Liu, X., Wang, J., Ge, W., Song, S., Dang, K., Wang, P., Wang, S., Tang, J., Zhong, H., Zhu, Y., Yang, M., Li, Z., Wan, J., Wang, P., Ding, W., Fu, Z., Xu, Y., Ye, J., Zhang, X., Xie, T., Cheng, Z., Zhang, H., Yang, Z., Xu, H., and Lin, J. Qwen2.5-vl technical report. *arXiv preprint arXiv:2502.13923*, 2025.
- Batra, H., Tu, H., Chen, H., Lin, Y., Xie, C., and Clark, R. Spatialthinker: Reinforcing 3d reasoning in multimodal llms via spatial rewards. *arXiv preprint arXiv:2511.07403*, 2025.
- Cai, W., Ponomarenko, I., Yuan, J., Li, X., Yang, W., Dong, H., and Zhao, B. Spatialbot: Precise spatial understanding with vision language models. In *2025 IEEE International Conference on Robotics and Automation (ICRA)*, pp. 9490–9498. IEEE, 2025a.
- Cai, Y., Li, K., Jia, M., Wang, J., Sun, J., Liang, F., Chen, W., Juefei-Xu, F., Wang, C., Thabet, A., et al. Phygdpo: Physics-aware groupwise direct preference optimization for physically consistent text-to-video generation. *arXiv preprint arXiv:2512.24551*, 2025b.
- Chen, B., Xu, Z., Kirmani, S., Ichter, B., Sadigh, D., Guibas, L., and Xia, F. Spatialvlm: Endowing vision-language models with spatial reasoning capabilities. In *Proceedings of the IEEE/CVF Conference on Computer Vision and Pattern Recognition (CVPR)*, pp. 14455–14465, 2024.
- Croitoru, F.-A., Hondru, V., Ionescu, R. T., Sebe, N., and Shah, M. Curriculum direct preference optimization for diffusion and consistency models. In *Proceedings of the Computer Vision and Pattern Recognition Conference (CVPR)*, pp. 2824–2834, 2025.
- Esser, P., Kulal, S., Blattmann, A., Entezari, R., Müller, J., Saini, H., Levi, Y., Lorenz, D., Sauer, A., Boesel, F., et al. Scaling rectified flow transformers for high-resolution image synthesis. In *Forty-first international conference on machine learning (ICML)*, 2024.
- Feng, W., Zhu, W., Fu, T.-j., Jampani, V., Akula, A., He, X., Basu, S., Wang, X. E., and Wang, W. Y. Layoutgpt: Compositional visual planning and generation with large language models. *Advances in Neural Information Processing Systems (NeurIPS)*, 36:18225–18250, 2023.
- Gordon, D., Kembhavi, A., Rastegari, M., Redmon, J., Fox, D., and Farhadi, A. Iqa: Visual question answering in interactive environments. In *Proceedings of the IEEE conference on computer vision and pattern recognition (CVPR)*, pp. 4089–4098, 2018.
- HaCohen, Y., Chiprut, N., Brazowski, B., Shalem, D., Moshe, D., Richardson, E., Levin, E., Shiran, G., Zabari, N., Gordon, O., et al. Ltx-video: Realtime video latent diffusion. *arXiv preprint arXiv:2501.00103*, 2024.
- He, W., Liu, M., Yu, Y., Wang, Z., and Wu, C. Dystxl: Dynamic layout planning and content control for compositional text-to-video generation. *arXiv preprint arXiv:2504.15032*, 2025.
- Hu, E. J., Shen, Y., Wallis, P., Allen-Zhu, Z., Li, Y., Wang, S., Wang, L., Chen, W., et al. Lora: Low-rank adaptation of large language models. *ICLR*, 1(2):3, 2022.
- Huang, Z., He, Y., Yu, J., Zhang, F., Si, C., Jiang, Y., Zhang, Y., Wu, T., Jin, Q., Chanpaisit, N., et al. Vbench: Comprehensive benchmark suite for video generative models. In *Proceedings of the IEEE/CVF Conference on Computer Vision and Pattern Recognition*, pp. 21807–21818, 2024.
- Hurst, A., Lerer, A., Goucher, A. P., Perelman, A., Ramesh, A., Clark, A., Ostrow, A., Welihinda, A., Hayes, A., Radford, A., et al. Gpt-4o system card. *arXiv preprint arXiv:2410.21276*, 2024.
- Karthik, S., Coskun, H., Akata, Z., Tulyakov, S., Ren, J., and Kag, A. Scalable ranked preference optimization for text-to-image generation. In *Proceedings of the IEEE/CVF International Conference on Computer Vision (ICCV)*, pp. 18399–18410, 2025.
- Li, R., Zheng, C., Rupprecht, C., and Vedaldi, A. Dso: Aligning 3d generators with simulation feedback for physical soundness. In *Proceedings of the IEEE/CVF International Conference on Computer Vision (ICCV)*, 2025.
- Li, Y., Liu, H., Wu, Q., Mu, F., Yang, J., Gao, J., Li, C., and Lee, Y. J. Gligen: Open-set grounded text-to-image generation. In *Proceedings of the IEEE/CVF conference on computer vision and pattern recognition (CVPR)*, pp. 22511–22521, 2023.
- Lian, L., Shi, B., Yala, A., Darrell, T., and Li, B. Llm-grounded video diffusion models. *arXiv preprint arXiv:2309.17444*, 2023.
- Liu, R., Wu, H., Zheng, Z., Wei, C., He, Y., Pi, R., and Chen, Q. Videodpo: Omni-preference alignment for video diffusion generation. In *Proceedings of the Computer Vision and Pattern Recognition Conference (CVPR)*, pp. 8009–8019, 2025.

- Loshchilov, I. and Hutter, F. Decoupled weight decay regularization. *arXiv preprint arXiv:1711.05101*, 2017.
- Ma, W., Chen, H., Zhang, G., Chou, Y.-C., Chen, J., de Melo, C., and Yuille, A. 3dsrbench: A comprehensive 3d spatial reasoning benchmark. In *Proceedings of the IEEE/CVF International Conference on Computer Vision (ICCV)*, pp. 6924–6934, 2025a.
- Ma, W., Chou, Y.-C., Liu, Q., Wang, X., de Melo, C., Xie, J., and Yuille, A. Spatialreasoner: Towards explicit and generalizable 3d spatial reasoning. *arXiv preprint arXiv:2504.20024*, 2025b.
- Na, S., Kim, Y., and Lee, H. Boost your human image generation model via direct preference optimization. In *Proceedings of the Computer Vision and Pattern Recognition Conference (CVPR)*, pp. 23551–23562, 2025.
- Oquab, M., Darcet, T., Moutakanni, T., Vo, H., Szafraniec, M., Khalidov, V., Fernandez, P., Haziza, D., Massa, F., El-Nouby, A., et al. Dinov2: Learning robust visual features without supervision. *arXiv preprint arXiv:2304.07193*, 2023.
- Ouyang, L., Wu, J., Jiang, X., Almeida, D., Wainwright, C., Mishkin, P., Zhang, C., Agarwal, S., Slama, K., Ray, A., et al. Training language models to follow instructions with human feedback. *Advances in neural information processing systems*, 35:27730–27744, 2022.
- Pal, A., Karkhanis, D., Dooley, S., Roberts, M., Naidu, S., and White, C. Smaug: Fixing failure modes of preference optimisation with dpo-positive. *CoRR*, abs/2402.13228, 2024. URL <https://doi.org/10.48550/arXiv.2402.13228>.
- Pang, R. Y., Yuan, W., He, H., Cho, K., Sukhbaatar, S., and Weston, J. Iterative reasoning preference optimization. *Advances in Neural Information Processing Systems (NeurIPS)*, 37:116617–116637, 2024.
- Peng, X., Zheng, Z., Shen, C., Young, T., Guo, X., Wang, B., Xu, H., Liu, H., Jiang, M., Li, W., Wang, Y., Ye, A., Ren, G., Ma, Q., Liang, W., Lian, X., Wu, X., Zhong, Y., Li, Z., Gong, C., Lei, G., Cheng, L., Zhang, L., Li, M., Zhang, R., Hu, S., Huang, S., Wang, X., Zhao, Y., Wang, Y., Wei, Z., and You, Y. Open-sora 2.0: Training a commercial-level video generation model in 200k. *arXiv preprint arXiv:2503.09642*, 2025.
- Qi, Z., Huang, G., Liu, C., and Ye, F. Layered rendering diffusion model for controllable zero-shot image synthesis. In *European Conference on Computer Vision*, pp. 426–443. Springer, 2024.
- Rafailov, R., Sharma, A., Mitchell, E., Manning, C. D., Ermon, S., and Finn, C. Direct preference optimization: Your language model is secretly a reward model. *Advances in Neural Information Processing Systems (NeurIPS)*, 36:53728–53741, 2023.
- Razin, N., Malladi, S., Bhaskar, A., Chen, D., Arora, S., and Hanin, B. Unintentional unalignment: Likelihood displacement in direct preference optimization. In *International Conference on Learning Representations (ICLR)*, 2025.
- Ren, T., Liu, S., Zeng, A., Lin, J., Li, K., Cao, H., Chen, J., Huang, X., Chen, Y., Yan, F., Zeng, Z., Zhang, H., Li, F., Yang, J., Li, H., Jiang, Q., and Zhang, L. Grounded sam: Assembling open-world models for diverse visual tasks, 2024.
- Schulman, J., Wolski, F., Dhariwal, P., Radford, A., and Klimov, O. Proximal policy optimization algorithms. *arXiv preprint arXiv:1707.06347*, 2017.
- Shao, Z., Wang, P., Zhu, Q., Xu, R., Song, J., Bi, X., Zhang, H., Zhang, M., Li, Y., Wu, Y., et al. Deepseekmath: Pushing the limits of mathematical reasoning in open language models. *arXiv preprint arXiv:2402.03300*, 2024.
- Team, Q. Qwen3 technical report, 2025a. URL <https://arxiv.org/abs/2505.09388>.
- Team, T. H. F. M. Hunyuanvideo 1.5 technical report, 2025b. URL <https://arxiv.org/abs/2511.18870>.
- Tian, Y., Yang, L., Yang, H., Gao, Y., Deng, Y., Chen, J., Wang, X., Yu, Z., Tao, X., Wan, P., et al. Videotetris: Towards compositional text-to-video generation. *Advances in Neural Information Processing Systems*, 37:29489–29513, 2024.
- Wallace, B., Dang, M., Rafailov, R., Zhou, L., Lou, A., Purushwalkam, S., Ermon, S., Xiong, C., Joty, S., and Naik, N. Diffusion model alignment using direct preference optimization. In *Proceedings of the IEEE/CVF Conference on Computer Vision and Pattern Recognition*, pp. 8228–8238, 2024.
- Wan, T., Wang, A., Ai, B., Wen, B., Mao, C., Xie, C.-W., Chen, D., Yu, F., Zhao, H., Yang, J., Zeng, J., Wang, J., Zhang, J., Zhou, J., Wang, J., Chen, J., Zhu, K., Zhao, K., Yan, K., Huang, L., Feng, M., Zhang, N., Li, P., Wu, P., Chu, R., Feng, R., Zhang, S., Sun, S., Fang, T., Wang, T., Gui, T., Weng, T., Shen, T., Lin, W., Wang, W., Wang, W., Zhou, W., Wang, W., Shen, W., Yu, W., Shi, X., Huang, X., Xu, X., Kou, Y., Lv, Y., Li, Y., Liu, Y., Wang, Y., Zhang, Y., Huang, Y., Li, Y., Wu, Y., Liu, Y., Pan, Y., Zheng, Y., Hong, Y., Shi, Y., Feng, Y., Jiang, Z., Han, Z., Wu, Z.-F., and Liu, Z. Wan: Open and

- advanced large-scale video generative models. *arXiv preprint arXiv:2503.20314*, 2025.
- Wang, J., Chan, K. C., and Loy, C. C. Exploring clip for assessing the look and feel of images. In *Proceedings of the AAAI conference on artificial intelligence*, volume 37, pp. 2555–2563, 2023.
- Wang, S., Lin, W., Huang, H., Wang, H., Cai, S., Han, W., Jin, T., Chen, J., Sun, J., Zhu, J., et al. Towards transformer-based aligned generation with self-coherence guidance. In *Proceedings of the Computer Vision and Pattern Recognition Conference*, pp. 18455–18464, 2025.
- Wang, X., Darrell, T., Rambhatla, S. S., Girdhar, R., and Misra, I. Instancediffusion: Instance-level control for image generation. In *Proceedings of the IEEE/CVF Conference on Computer Vision and Pattern Recognition (CVPR)*, pp. 6232–6242, 2024.
- Wu, Q., Teney, D., Wang, P., Shen, C., Dick, A., and Van Den Hengel, A. Visual question answering: A survey of methods and datasets. *Computer Vision and Image Understanding (CVIU)*, 163:21–40, 2017.
- Wu, T.-H., Lian, L., Gonzalez, J. E., Li, B., and Darrell, T. Self-correcting llm-controlled diffusion models. In *Proceedings of the IEEE/CVF Conference on Computer Vision and Pattern Recognition*, pp. 6327–6336, 2024.
- Xie, J., Li, Y., Huang, Y., Liu, H., Zhang, W., Zheng, Y., and Shou, M. Z. Boxdiff: Text-to-image synthesis with training-free box-constrained diffusion. In *Proceedings of the IEEE/CVF International Conference on Computer Vision*, pp. 7452–7461, 2023.
- Xu, P., Wang, S., Zhu, Y., Li, J., and Zhang, Y. Spatialbench: Benchmarking multimodal large language models for spatial cognition. *arXiv preprint arXiv:2511.21471*, 2025.
- Yang, L., Yu, Z., Meng, C., Xu, M., Ermon, S., and Cui, B. Mastering text-to-image diffusion: Recaptioning, planning, and generating with multimodal llms. In *Forty-first International Conference on Machine Learning*, 2024.
- Yang, X., Tan, Z., and Li, H. Ipo: Iterative preference optimization for text-to-video generation. *arXiv preprint arXiv:2502.02088*, 2025a.
- Yang, Z., Teng, J., Zheng, W., Ding, M., Huang, S., Xu, J., Yang, Y., Hong, W., Zhang, X., Feng, G., et al. Cogvideox: Text-to-video diffusion models with an expert transformer. In *International Conference on Learning Representations (ICLR)*, 2025b.
- Zheng, D., Huang, Z., Liu, H., Zou, K., He, Y., Zhang, F., Zhang, Y., He, J., Zheng, W.-S., Qiao, Y., et al. Vbench-2.0: Advancing video generation benchmark suite for

Supplemental Material

A1. Additional Experimental Settings

A1.1. Metrics

Correctness We use the DSR-SCORE defined in Section 3.2 to measure how well the generated video aligns with the dynamic spatial relationship (DSR) described in the prompt. In particular, we count the *percentage* of samples in the test set having $\text{DSR-SCORE} \geq \tau_{\text{test}}$ as the correctness (denoted as $\text{Correctness@}\tau_{\text{test}}$) of DSR. Intuitively, it indicates the rate where the T2V model can produce DSR samples up to a certain level of quality, reflecting the model’s general ability to align with DSR prompts. At $\tau_{\text{test}} = 0$, correctness is validness, reflecting the percentage of valid samples among the total number of test samples. We particularly focus on Correctness@0.7 , effectively having $\tau_{\text{test}} = \tau_{\text{train}}$. In addition to the single Correctness@0.7 value, we also check the *correctness curve*, which is the correctness at varied $\tau_{\text{test}} \in [0, 1]$.

ID Consistency We aim to measure the consistency of the animal appearance along the video frames. VBench (Huang et al., 2024) measures subject consistency by checking the DINOv2 (Oquab et al., 2023) feature similarity of the frames with respect to the first frame and the previous frame. However, the calculation is based on the whole frame, where the background is involved. In order to have a more precise assessment of the consistency of the *animal*, we only extract DINOv2 features within the bounding box containing the animal for the similarity measurement.

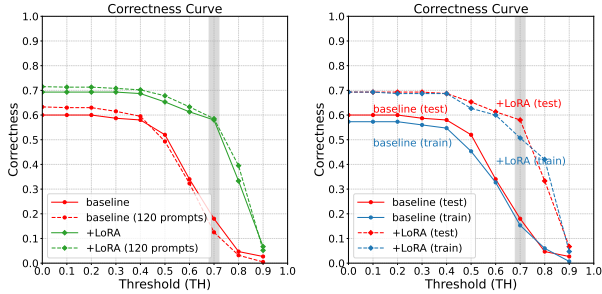
CLIP-IQA and Imaging Quality We use CLIP-IQA (Wang et al., 2023) and Imaging Quality (from VBench (Huang et al., 2024)) to collectively assess the visual quality of the generated samples. For CLIP-IQA, we compute at the “natural” mode on the video frames and take average. A higher CLIP-IQA “natural” score means that the video frame is more likely classified as “*Natural photo*” than “*Synthetic photo*”. For Imaging Quality, we follow VBench (Huang et al., 2024) to extract the DINOv2 (Oquab et al., 2023) feature for the whole frame, and compute the sharpness and colorfulness. A higher Imaging Quality score means that the video frame is sharper and more colorful. For both CLIP-IQA and Imaging Quality, we take the average score on all frames as the final score for the video.

A1.2. Examples of our curated DSR-DATASET

- On a grassy field with wildflowers, a rabbit is on the left of a stone, then the rabbit jumps to the right of the stone.
- In a quiet forest clearing, a squirrel is on the left of a lamp,

then the squirrel scampers to the right of the lamp.

- By a calm riverbank with reeds, a cat is on the left of a hydrant, then the cat paces to the right of the hydrant.
- At the edge of a sunny meadow, a dog is on the left of a bucket, then the dog runs to the right of the bucket.
- On a rocky hillside with moss, a fox is on the left of a chair, then the fox sprints to the right of the chair.
- At a seaside dock with gulls, a turtle is on the left of a bench, then the turtle ambles to the top of the bench.
- Near a market square with stalls, a rabbit is on the left of a crate, then the rabbit hops to the top of the crate.
- On a plaza with stone benches, a squirrel is on the left of a stone, then the squirrel darts to the top of the stone.
- Inside a hallway with framed photos, a cat is on the left of a lamp, then the cat sneaks to the top of the lamp.
- By a village well with buckets, a dog is on the left of a chair, then the dog trots to the top of the chair.
- On a breezy hilltop at dusk, a cat is on the right of a hydrant, then the cat prowls to the left of the hydrant.
- In a maple grove with red leaves, a dog is on the right of a bucket, then the dog bounds to the left of the bucket.
- By a pebble beach with driftwood, a fox is on the right of a chair, then the fox dashes to the left of the chair.
- At a fountain plaza with tiles, a bird is on the right of a bench, then the bird flutters to the left of the bench.
- Inside a sunroom with potted plants, a duck is on the right of a crate, then the duck shuffles to the left of the crate.
- At a gazebo with benches, a squirrel is on the right of a stone, then the squirrel scampers to the top of the stone.
- On a slope with stepping stones, a cat is on the right of a lamp, then the cat paces to the top of the lamp.
- By a trailhead signpost, a dog is on the right of a chair, then the dog runs to the top of the chair.
- In a colonnade with pillars, a fox is on the right of a bench, then the fox sprints to the top of the bench.
- At a riverside promenade with lamps, a bird is on the right of a crate, then the bird pecks to the top of the crate.
- At a pergola featuring climbing vines, a monkey is on the top of a log, then the monkey leaps to the left of the log.
- At a pergola showing climbing vines, a turtle is on the top of a bench, then the turtle shuffles to the left of the bench.
- Inside a gallery featuring white walls, a rabbit is on the top of a stone, then the rabbit jumps to the left of the stone.
- Inside a gallery showing white walls, a squirrel is on the top of a desk, then the squirrel scampers to the left of the desk.
- On a courtyard deck featuring lanterns, a cat is on the top of a table, then the cat paces to the left of the table.



(a) Main result on Wan2.1-1.3B (b) Test set vs. Train set (subset)

Figure A6. **Correctness curve.** The percentage of samples having DSR-SCORE $\geq \tau_{\text{test}}$ under different τ_{test} . The emphasized focus (grey area) is on $\tau_{\text{test}} = 0.7$. (a) The training significantly enhances the model’s ability in aligning with DSR prompts. (b) We compare the result on the test set to a subset of training set (also 30 prompts), and indicate that the fine-tuned model is not overfit to the training set.

- On a courtyard deck showing lanterns, a squirrel is **on the top** of a stone, then the squirrel darts **to the right** of the stone.
- Near a hedgerow featuring sparrows, a cat is **on the top** of a desk, then the cat sneaks **to the right** of the desk.
- Near a hedgerow showing sparrows, a dog is **on the top** of a bench, then the dog trots **to the right** of the bench.
- By a canal featuring brick edges, a fox is **on the top** of a chair, then the fox trots **to the right** of the chair.
- By a canal showing brick edges, a bird is **on the top** of a crate, then the bird hops **to the right** of the crate.

A2. Additional Analysis

Ablations on the training set. DPO is prone to overfitting due its offline nature of training on collected data, compared to PPO/GRPO which are trained on online data. To investigate whether our fine-tuned model has overfit to the training set, we selected a subset of 30 prompts from the training set for testing. As shown in Figure A6b, the fine-tuned model demonstrates a similar performance enhancement on this training subset as that on the test set. This indicates that the overfitting is not significantly observed and our method appears to have acquired semantic-level understanding of spatial relationships.

Analysis of Internal Changes in Text-to-Latent Attention. Apart from monitoring the performance enhancement, it is also essential to analyze the internal changes caused by the fine-tuning. Here we investigate the angle of *text-to-latent* correlation. Since the model has a classical *cross-attention* design whereby the text tokens (tokenized from the prompt) attend to the video latents, we consider the patterns in the *cross-attention activation map* (CAMAP) to be reflective of the text-to-latent correlation.

		Animal	Object	Initial SSR	Final SSR	Others
Baseline	Initial SSR	0.395	0.280	1.000	0.837	0.878
	Final SSR	0.435	0.278	0.837	1.000	0.892
+ LoRA	Initial SSR	0.456	0.277	1.000	0.866	0.894
	Final SSR	0.489	0.274	0.866	1.000	0.903

Table A5. **CAMAP Analysis.** We compute the average CAMAP correlation between different types of tokens: Animal-related tokens, Object-related tokens, Initial SSR-related tokens, Final SSR-related tokens, and Other tokens. The fine-tuned model shows a stronger correlation between the $\langle \text{initial SSR} \rangle$ -to- $\langle \text{animal} \rangle$ and $\langle \text{final SSR} \rangle$ -to- $\langle \text{animal} \rangle$ pairs, indicating better capturing of the spatial relationships specified in the DSR prompts.

In particular, we focus on the *similarity* between the CAMAP values (flattened as a vector) of the tokens for initial/final SSR with respect to the $\langle \text{animal} \rangle$ and the $\langle \text{static object} \rangle$ tokens. This approach is taken because SSR is not a tangible concept like $\langle \text{animal} \rangle$ or $\langle \text{static object} \rangle$ that is directly reflected in the geometrical patterns within CAMAP, but rather has a modifier effect. The similarity in CAMAP reflects the strength of binding between the SSR tokens and $\langle \text{animal} \rangle / \langle \text{static object} \rangle$.

As shown in Table A5, we split the prompt into 5 groups and inspect the similarity of CAMAP values between the initial/final SSR group and the 5 groups. Comparing the baseline and the fine-tuned model, significantly increased correlation occurs for $\langle \text{initial SSR} \rangle$ -to- $\langle \text{animal} \rangle$ and $\langle \text{final SSR} \rangle$ -to- $\langle \text{animal} \rangle$. This provides some evidence that our method takes effect by making the tokens of initial/final SSR more tightly bound to the tokens of $\langle \text{animal} \rangle$.

Ablations on the loss setting with training curves. This is an extension of Figure 3 and Section 4.3 in the main paper. We show the training curves of DPO loss \mathcal{L}_{DPO} and with the regularization losses \mathcal{L}_{ZO} in Figure A7. It can be observed that with only DPO loss, the training is unstable and the loss fluctuates heavily. With our zeroth-order regularization, the DPO process exhibits more stable training.

A3. Correctness Curves of Ablation Studies

We show the correctness curves of the ablation studies discussed in Section 4.3 to convey additional information beyond the singular values provided in the main paper.

Figures A8a and A8b show the ablation under different training losses. Our setting of doing DPO with τ_{train} shows a clear advantage over SFT/DPO w/o τ_{train} . As for the choice of regularization loss, our \mathcal{L}_{ZO} performs better than \mathcal{L}_{SFT} as the training progresses to 2400 steps.

Figure A8d shows the ablation on different τ_{train} for splitting the winner/loser training samples. As τ_{train} goes from 0.6 to 0.8, an overall shift is witnessed across all τ_{test} . This shows that our DSR-SCORE can serve as a stable and progressive

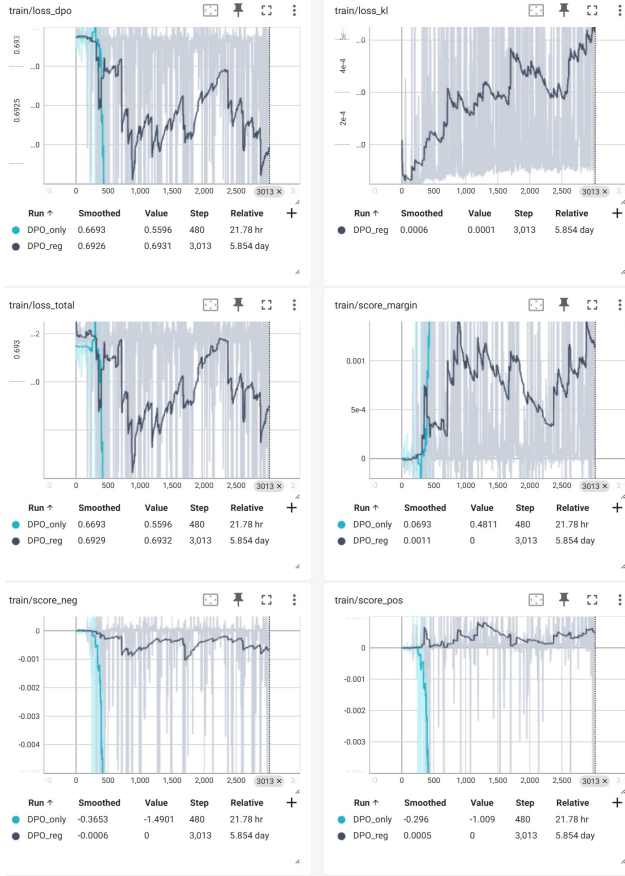


Figure A7. Training curves of $\mathcal{L}_{DPO} + \lambda_{ZO}\mathcal{L}_{ZO}$ (black) and \mathcal{L}_{DPO} (blue). With only \mathcal{L}_{DPO} , the training exhibits *likelihood displacement*: the winner-side implicit reward $score_pos$ drops catastrophically and the loser-side reward $score_neg$ drops even further, raising up the $score_margin$ in an incorrect way. In contrast, the existence of \mathcal{L}_{ZO} keeps $score_pos$ at slight growth and $score_neg$ at slight drop, giving a healthier growing of $score_margin$.

optimization signal.

Figures A8c and A8e show the ablation using different reward systems. With only endpoint values, fine-tuning is unable to reach the same level of performance as using the full DSR-SCORE. Compared to VLM-based evaluation, our DSR-SCORE gives a much better performance, suggesting that our metric is more reliable in terms of providing an optimization signal for fine-tuning.

Figure A8f shows the result of testing on different prompt structures, despite only fine-tuning our model with a specific prompt structure. For all three types of alternative prompts, the fine-tuned model performs better than the baseline. This suggests that the fine-tuned model has acquired some semantic knowledge about spatial relationships, rather than simply overfitting to the training prompts.

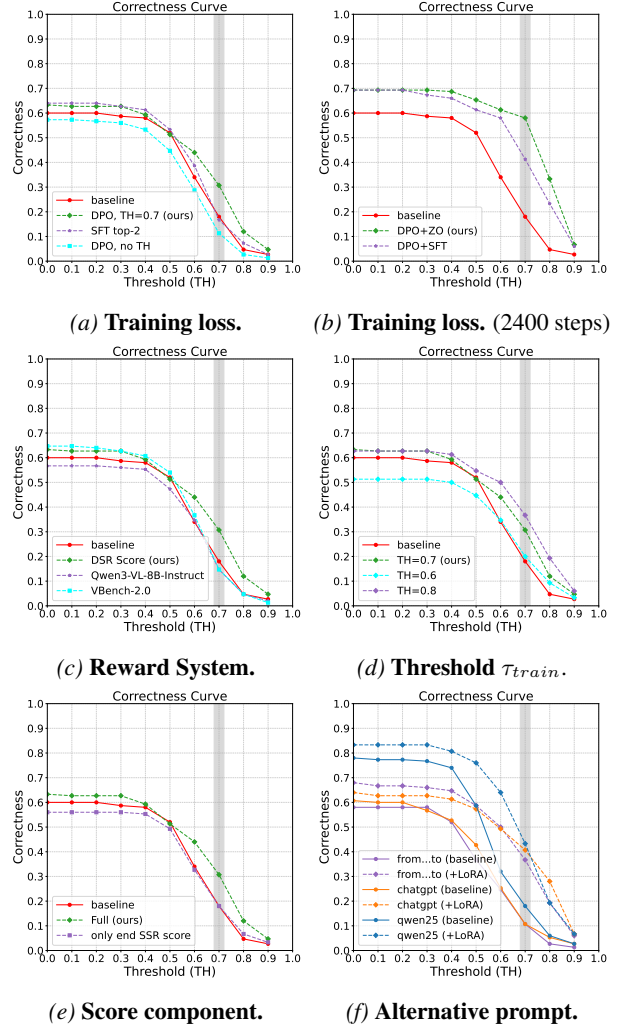


Figure A8. Ablation Studies. This is an extended version of Table 4 in the main paper, showing the correctness curves of various ablations.

A4. Theoretical Analysis of the Regularization Term \mathcal{L}_{ZO}

The original DPO loss is

$$\mathcal{L}_{DPO}(\theta) = -\mathbb{E}_{(p, x^w, x^l, t)} \left[\log \sigma \left(\beta \left(\begin{aligned} & (\|\epsilon^w - \epsilon_{\theta}(x_t^w, t)\|_2^2 - \|\epsilon^w - \epsilon_{\text{ref}}(x_t^w, t)\|_2^2) \\ & - (\|\epsilon^l - \epsilon_{\theta}(x_t^l, t)\|_2^2 - \|\epsilon^l - \epsilon_{\text{ref}}(x_t^l, t)\|_2^2) \end{aligned} \right) \right) \right] \quad (1)$$

Denote

$$A_\theta^w = \|\epsilon^w - \epsilon_\theta(x_t^w, t)\|_2^2 - \|\epsilon^w - \epsilon_{\text{ref}}(x_t^w, t)\|_2^2 \quad (2)$$

$$A_\theta^l = \|\epsilon^l - \epsilon_\theta(x_t^l, t)\|_2^2 - \|\epsilon^l - \epsilon_{\text{ref}}(x_t^l, t)\|_2^2 \quad (3)$$

$$z = \beta(A_\theta^w - A_\theta^l) \quad (4)$$

$$\mathcal{L}_{\text{DPO}}(\theta) = -\mathbb{E}[\log \sigma(z)] \quad (5)$$

then the gradient of the DPO loss is

$$\nabla_\theta \mathcal{L}_{\text{DPO}}(\theta) = -\mathbb{E}[(1 - \sigma(z)) \nabla_\theta z] \quad (6)$$

where the gradient $\nabla_\theta z$ is

$$\nabla_\theta z = \beta(\nabla_\theta A_\theta^w - \nabla_\theta A_\theta^l) \quad (7)$$

$$\nabla_\theta A_\theta^w = 2(\nabla_\theta \epsilon_\theta(x_t^w, t))^\top (\epsilon_\theta(x_t^w, t) - \epsilon^w) \quad (8)$$

$$\nabla_\theta A_\theta^l = 2(\nabla_\theta \epsilon_\theta(x_t^l, t))^\top (\epsilon_\theta(x_t^l, t) - \epsilon^l) \quad (9)$$

Denote

$$J^w = \nabla_\theta \epsilon_\theta(x_t^w, t), \quad J^l = \nabla_\theta \epsilon_\theta(x_t^l, t) \quad (10)$$

$$\delta^w = \delta_\theta(x_t^w, t) = \epsilon_\theta(x_t^w, t) - \epsilon_{\text{ref}}(x_t^w, t) \quad (11)$$

$$\delta^l = \delta_\theta(x_t^l, t) = \epsilon_\theta(x_t^l, t) - \epsilon_{\text{ref}}(x_t^l, t) \quad (12)$$

At the neighborhood of ϵ_{ref}

$$\mathbb{E}[\epsilon - \epsilon_{\text{ref}}(x_t, t)] = 0 \quad (13)$$

then

$$\delta^w \approx \epsilon_\theta(x_t^w, t) - \epsilon^w, \quad \delta^l \approx \epsilon_\theta(x_t^l, t) - \epsilon^l \quad (14)$$

and the gradient can be written as

$$\nabla_\theta z = \beta(\nabla_\theta A_\theta^w - \nabla_\theta A_\theta^l) \approx 2\beta((J^w)^\top \delta^w - (J^l)^\top \delta^l) \quad (15)$$

The regularization loss is

$$\begin{aligned} \mathcal{L}_{\text{ZO}}(\theta) = \mathbb{E}_{(p, x^w, x^l, t)} & \left[\|\epsilon_\theta(x_t^w, t) - \epsilon_{\text{ref}}(x_t^w, t)\|_2^2 \right. \\ & \left. + \|\epsilon_\theta(x_t^l, t) - \epsilon_{\text{ref}}(x_t^l, t)\|_2^2 \right] \end{aligned} \quad (16)$$

its gradient is

$$\begin{aligned} \nabla_\theta \mathcal{L}_{\text{ZO}} = 2\mathbb{E} & \left[(\nabla_\theta \epsilon_\theta(x_t^w, t))^\top (\epsilon_\theta(x_t^w, t) - \epsilon_{\text{ref}}(x_t^w, t)) + \right. \\ & \left. (\nabla_\theta \epsilon_\theta(x_t^l, t))^\top (\epsilon_\theta(x_t^l, t) - \epsilon_{\text{ref}}(x_t^l, t)) \right] \end{aligned} \quad (17)$$

With $J^w, J^l, \delta^w, \delta^l$, we have

$$\nabla_\theta \mathcal{L}_{\text{ZO}} = 2\mathbb{E}[(J^w)^\top \delta^w + (J^l)^\top \delta^l] \quad (18)$$

Denote

$$\delta^S = \frac{1}{2}(\delta^w + \delta^l), \quad \delta^D = \frac{1}{2}(\delta^w - \delta^l),$$

$$J^S = \frac{1}{2}(J^w + J^l), \quad J^D = \frac{1}{2}(J^w - J^l) \quad (19)$$

Then the two gradient can be written as

$$\begin{aligned} \nabla_\theta z & \approx 2\beta((J^w)^\top \delta^w - (J^l)^\top \delta^l) \\ & = 4\beta((J^S)^\top \delta^D + (J^D)^\top \delta^S) \end{aligned} \quad (20)$$

$$\begin{aligned} \nabla_\theta \mathcal{L}_{\text{ZO}} & = 2\mathbb{E}[(J^w)^\top \delta^w + (J^l)^\top \delta^l] \\ & = 4\mathbb{E}[(J^S)^\top \delta^S + (J^D)^\top \delta^D] \end{aligned} \quad (21)$$

Given the same prompt and the same denoising timestep t , the two samples x^w and x^l are located within a neighborhood, making J^w close to J^l in terms of norm. This is even consolidated under the low-rank adaption (LoRA) setting of optimization. Therefore, the common component $J^S = \frac{1}{2}(J^w + J^l)$ should be dominant over $J^D = \frac{1}{2}(J^w - J^l)$ in terms of norm.

In the gradient of DPO $\nabla_\theta z$, J^S amplifies the difference part δ^D , leading to a shift towards x^w . However, the common part δ^S is not amplified at the same level, since J^D is rather small. This undermines the foundation level of alignment to the prompt. In fact, when we want to shift the model distribution towards the preferred samples, an implicit assumption is that the basic level of alignment to both preferred and unwanted samples should be maintained.

In the gradient of \mathcal{L}_{ZO} , the common part δ^S is reserved by the dominant component J^S , **counteracting** the risk of ‘‘losing the common ground’’ induced in $\nabla_\theta z$, which helps to maintain the stability at a coefficient λ_{ZO} .

If \mathcal{L}_{ZO} only constrains the win part ϵ_θ^w , then the gradient will be

$$(J^S)^\top \delta^S + (J^S)^\top \delta^D + (J^D)^\top \delta^S + (J^D)^\top \delta^D \quad (22)$$

which contains some part of $\nabla_\theta z$ and the alleviation is not as effective.

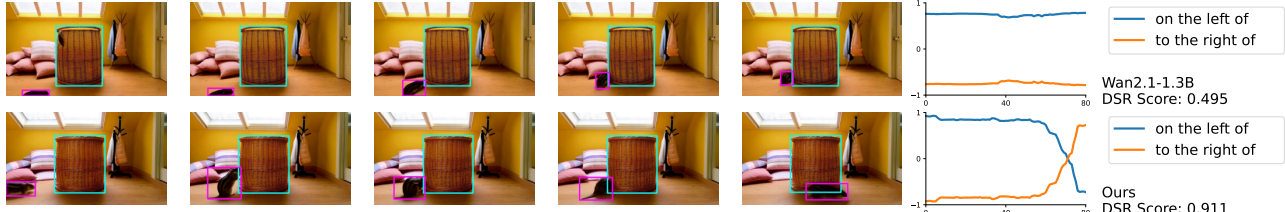
A5. More Qualitative Results

(see next page)

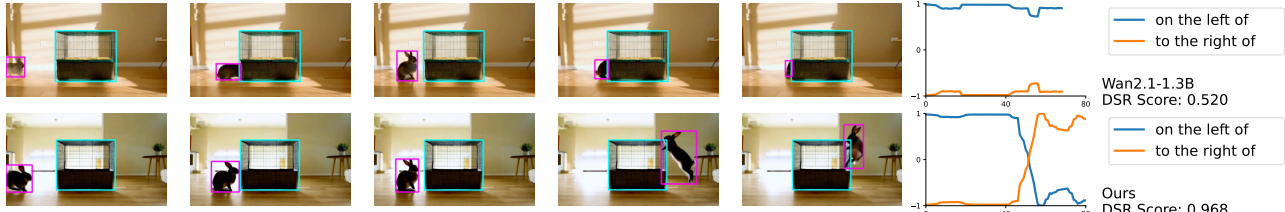
On a grassy field with wildflowers, a rabbit is on the left of a stone, then the rabbit jumps to the right of the stone.



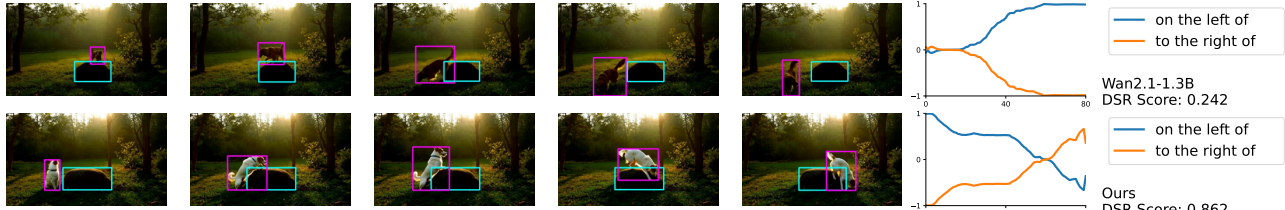
In a sunlit loft space with pillows on the floor and a coat rack by the door, a hamster is on the left of a basket, then the hamster scurries to the right of the basket.



In a spacious living room with a low table and sunlight spilling across the floor, a rabbit is on the left of a crate, then the rabbit jumps to the right of the crate.



In an open shady grove with distant trees in the background and hazy light filtering through the trees, a dog is on the left of a stone, then the dog trots to the right of the stone.



In a sunlit dusty path with soft soil underfoot and the sound of water somewhere nearby, a cat is on the left of a stump, then the cat walks to the right of the stump.



At the edge of a sunny meadow, a dog is on the left of a bucket, then the dog runs to the right of the bucket.

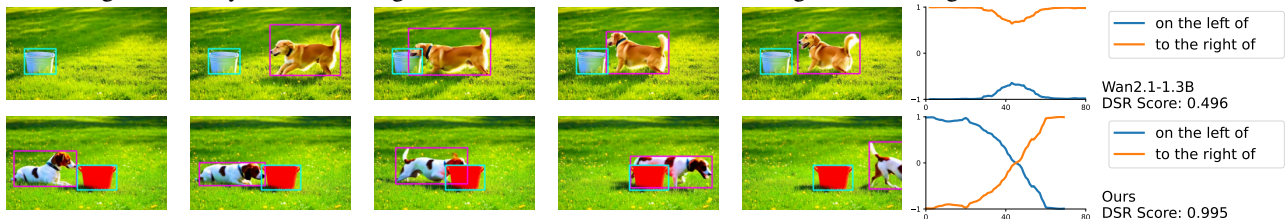
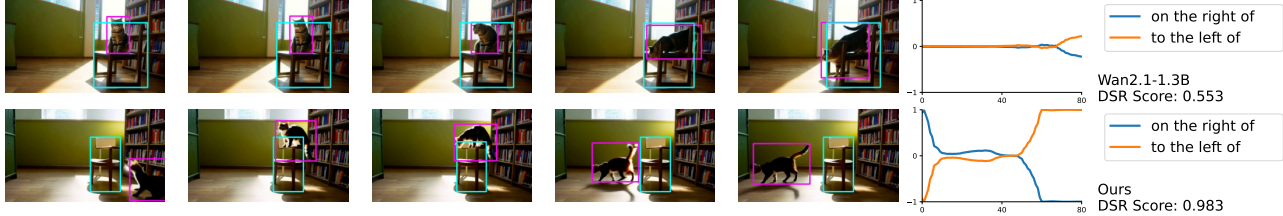


Figure A9. Qualitative results set1.

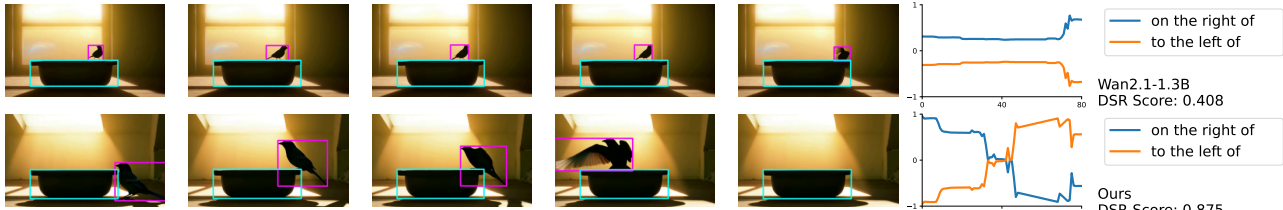
Inside a sunroom with potted plants, a duck is on the right of a crate, then the duck shuffles to the left of the crate.



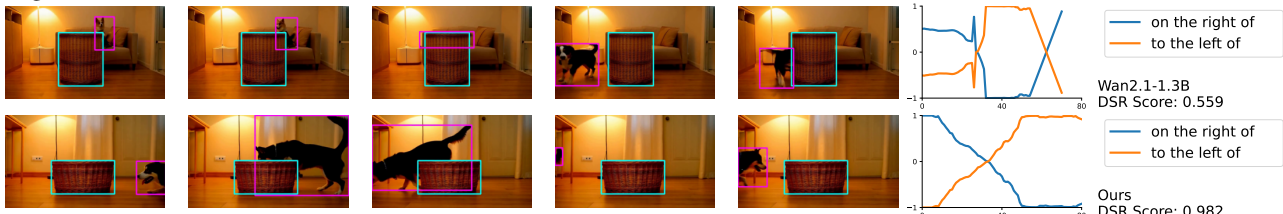
In a spacious library corner with a large window and sunlight spilling across the floor, a cat is on the right of a chair, then the cat walks to the left of the chair.



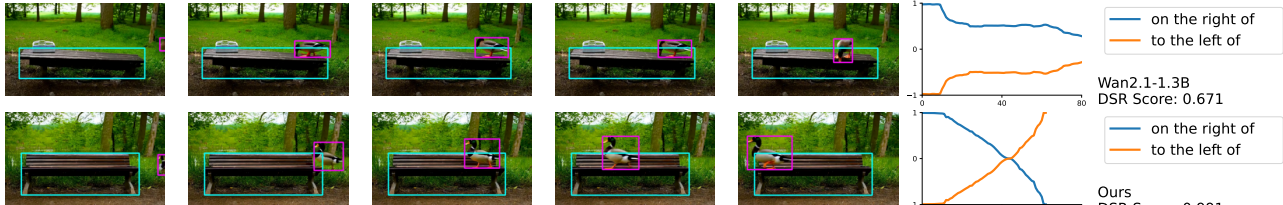
In a softly lit loft space with a large window and sunlight spilling across the floor, a bird is on the right of a pot, then the bird hops to the left of the pot.



In a softly lit living room with wooden floors and warm light from a nearby lamp, a dog is on the right of a basket, then the dog runs to the left of the basket.



In a quiet campsite with shadows from nearby trees and quiet air with almost no wind, a duck is on the right of a bench, then the duck waddles to the left of the bench.

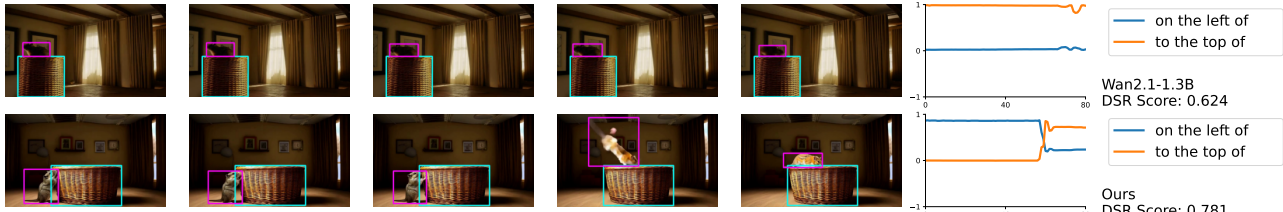


In an open campsite with tall grass swaying gently and quiet air with almost no wind, a fox is on the right of a bench, then the fox walks to the left of the bench.



Figure A10. Qualitative results set2.

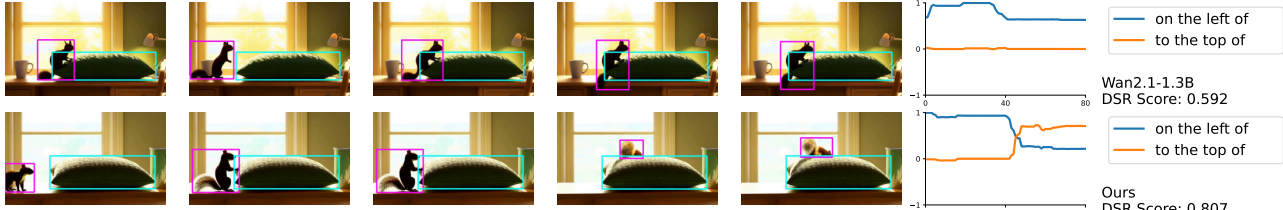
In a spacious loft space with framed pictures and heavy curtains drawn halfway, a hamster is on the left of a basket, then the hamster climbs to the top of the basket.



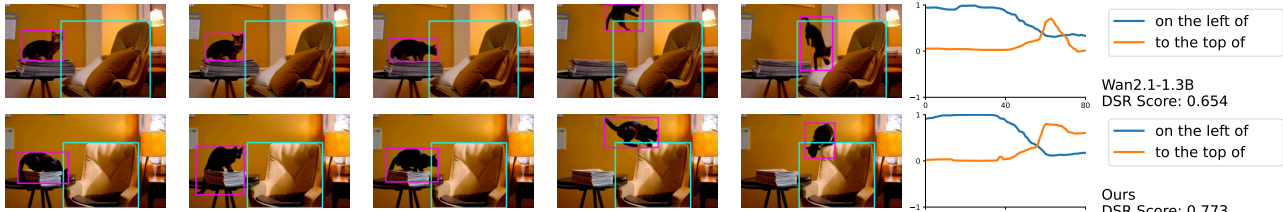
In a narrow attic with a floor lamp and shadows from the window blinds, a hamster is on the left of a box, then the hamster climbs to the top of the box.



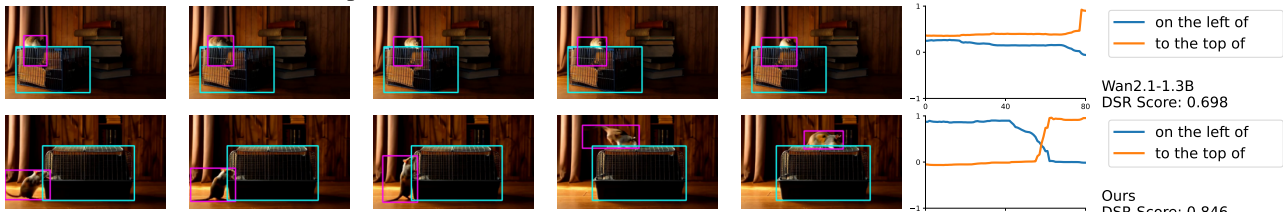
In a sunlit office with a large window and a mug left on a side table, a squirrel is on the left of a cushion, then the squirrel darts to the top of the cushion.



In a warm office with soft cushions and a stack of magazines on a table, a cat is on the left of a chair, then the cat jumps to the top of the chair.



In a wood-paneled storage room with scattered books and heavy curtains drawn halfway, a hamster is on the left of a crate, then the hamster climbs to the top of the crate.



In a quiet shady grove with distant trees in the background and long shadows as the sun sits low, a dog is on the left of a stump, then the dog jumps to the top of the stump.

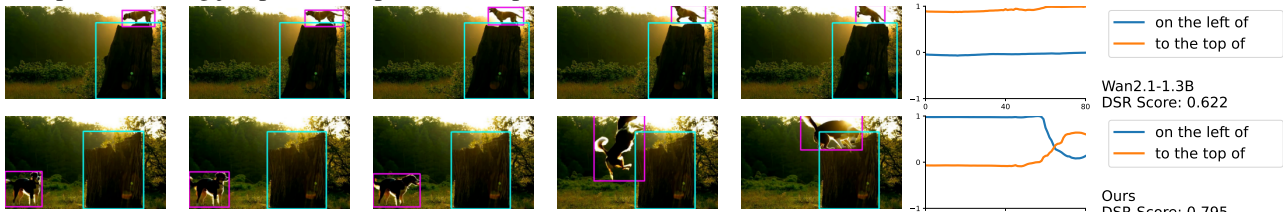
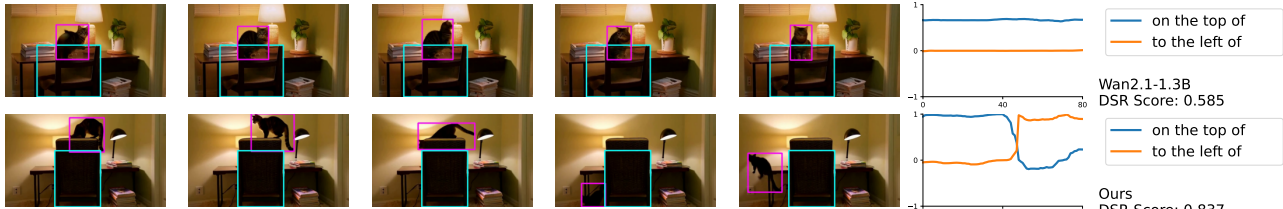


Figure A11. Qualitative results set3.

At a pergola showing climbing vines, a turtle is on the top of a bench, then the turtle shuffles to the left of the bench.



In a quiet reading nook with a floor lamp and a stack of magazines on a table, a cat is on the top of a chair, then the cat jumps to the left of the chair.



In a misty forest clearing with distant trees in the background and quiet air with almost no wind, a fox is on the top of a stump, then the fox jumps to the left of the stump.



In a sloping shady grove with tall grass swaying gently and birds faintly calling in the distance, a hamster is on the top of a bench, then the hamster scurries to the left of the bench.



In a sloping park lawn with distant trees in the background and distant hills on the horizon, a fox is on the top of a stump, then the fox jumps to the left of the stump.

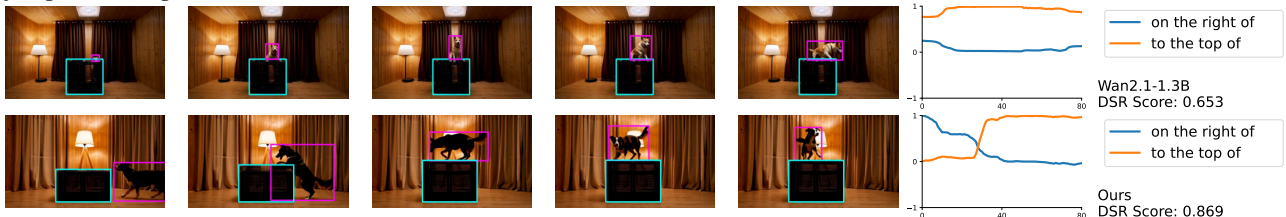


In a sunlit rocky shore with fallen leaves on the ground and the sound of water somewhere nearby, a squirrel is on the top of a stump, then the squirrel darts to the left of the stump.

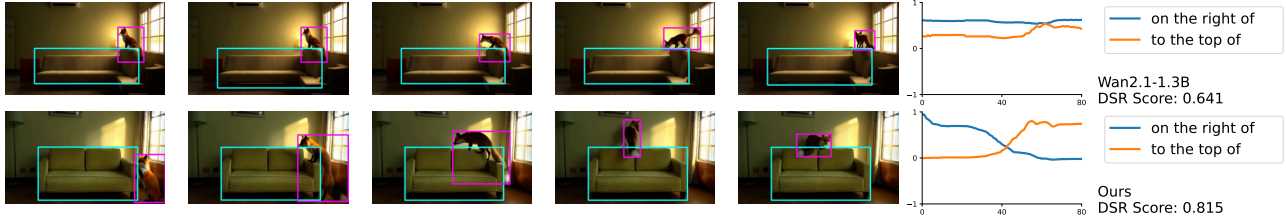


Figure A12. Qualitative results set4.

In a wood-paneled studio with a floor lamp and heavy curtains drawn halfway, a dog is on the right of a crate, then the dog jumps to the top of the crate.



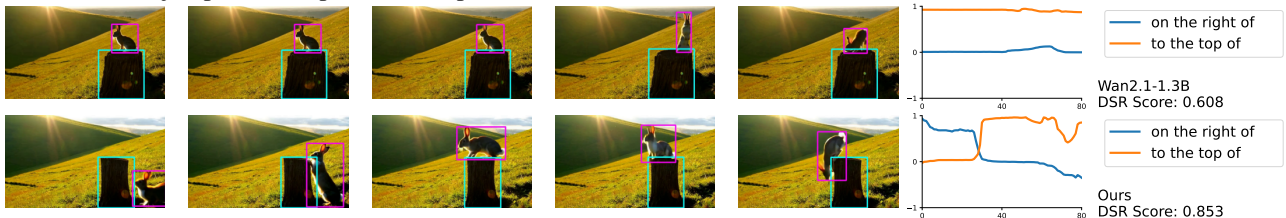
In a softly lit storage room with a large window and a single lamp in the corner, a fox is on the right of a sofa, then the fox trots to the top of the sofa.



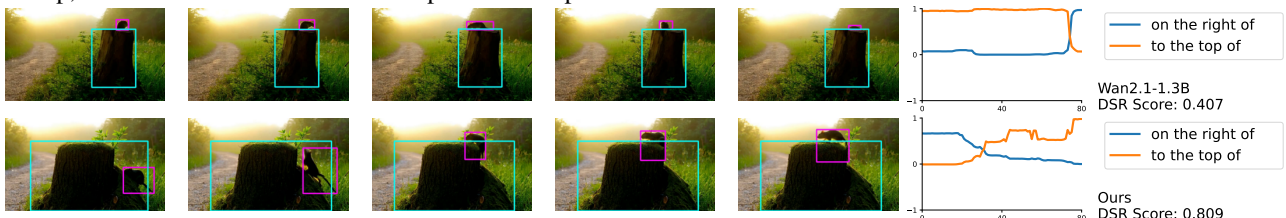
In a sloping garden path with a few bushes near the edge and long shadows as the sun sits low, a rabbit is on the right of a bench, then the rabbit jumps to the top of the bench.



In a sunlit hillside slope with patches of bare earth and long shadows as the sun sits low, a rabbit is on the right of a stump, then the rabbit jumps to the top of the stump.



In a misty woodland trail with a few bushes near the edge and long shadows as the sun sits low, a hamster is on the right of a stump, then the hamster hurries to the top of the stump.

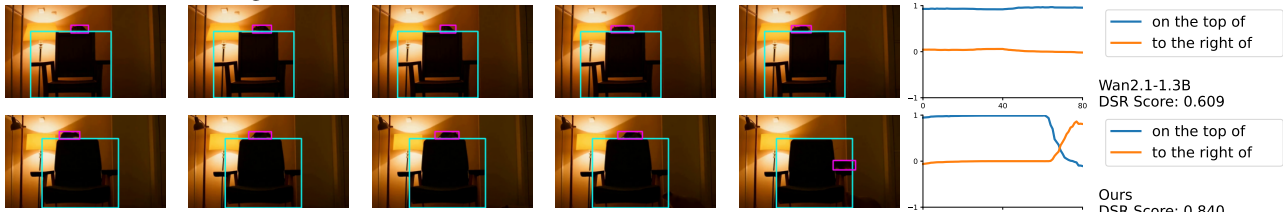


In a peaceful woodland trail with small rocks underfoot and a cool breeze moving the grass, a cat is on the right of a stone, then the cat prowls to the top of the stone.

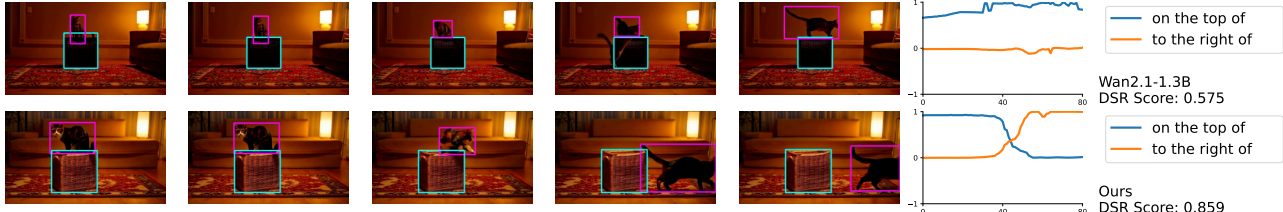


Figure A13. Qualitative results set5.

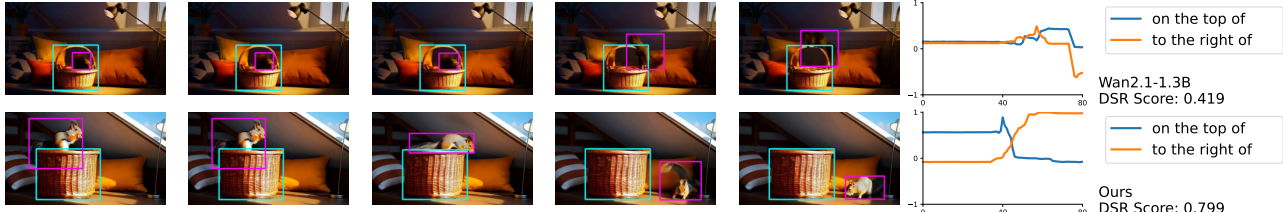
In a softly lit storage room with a floor lamp and warm light from a nearby lamp, a hamster is on the top of a chair, then the hamster crawls to the right of the chair.



In a warm living room with a patterned rug and warm light from a nearby lamp, a cat is on the top of a crate, then the cat jumps to the right of the crate.



In a sunlit attic with soft cushions and warm light from a nearby lamp, a squirrel is on the top of a basket, then the squirrel jumps to the right of the basket.



In an open campsite with tall grass swaying gently and clouds drifting slowly by, a hamster is on the top of a rock, then the hamster crawls to the right of the rock.



In a quiet meadow with distant trees in the background and hazy light filtering through the trees, a squirrel is on the top of a rock, then the squirrel leaps to the right of the rock.



In a windy grassy field with distant trees in the background and quiet air with almost no wind, a fox is on the top of a rock, then the fox dashes to the right of the rock.



Figure A14. Qualitative results set6.